Memoirs of the Faculty of Engineering, Nagoya University
Vol.43, No.1 (1991)

STUDIES ON THE LIQUID MEMBRANE SEPARATION OF METAL CATIONS USING MOBILE CARRIER

Hiroshi TAKEUCHI

Department of Chemical Engineering

(Received May 31, 1991)

Abstract

Liquid membrane separation, which combines the solvent extraction and stripping processes in a single step, has been an area deserving special attention because of it great potential for low cost and energy saving. In this article, we reviewed our previous works on two kinds of liquid membranes: supported liquid membranes (SLM), immobilized on microporous polymeric membrane, and emulsifying liquid membranes (ELM) as a $(W/O)/W$ emulsion. Transport of metal ions across SLM is formulated on the basis of mass-transfer processes including the interfacial chemical reaction. In addition, stabilities of both membranes of SLM and ELM are described, and the countermeasures for assuring the possible operating stability have been considered. Finally, the applications of SLM to the separation and concentration of cations were illustrated for aqueous solutions of some alkaline and heavy metal ions.

Contents

1. Introduction 55
2. Permeation rates across liquid membranes 56
2. 1. Aqueous film mass-transfer coefficient 56
2. 1. 1. Flat-type membrane module 58
2. 1. 2. Hollow-fiber module 59
2. 2. Membrane-transfer coefficient 63
2. 2. 1. Effective diffusivity 63
2. 2. 2. Effective diffusion-length and interfacial area 65
2. 3. Interfacial chemical reaction 67
2. 3. 1. Extraction of copper by LIX65*N* 67
2. 3. 2. Extraction of chromium (VI) by *3*-(*4*-pyridyl)-*1,5*-diphenyl pentane 70

2. 3. 3. Extraction equilibria of di- and tri-valent metal ions by 2-ethylhexyl phosphonic acid mono-(2-ethylhexyl) ester 74
2. 3. 4. Extraction of cadmium (II) by D2EHPA 75
2. 3. 5. Extraction of gallium (III) by PC-88A 78
2. 3. 6. Extraction of Ti(IV) from acid media by D2EHPA 78
2. 4. Permeation rate of cadmium (II) across an SLM containing D2EHPA 80
3. Stabilities of liquid membranes 82
3. 1. Supported liquid membrane (SLM) 82
3. 1. 1. Breakdown time of SLMs 83
3. 1. 2. Mechanism of SLM breakdown 85
3. 1. 3. Progressive wetting of SLMs by aqueous solutions 86
3. 2. Methods for continuous regeneration of SLMs 88
3. 2. 1. Mixed flow mode of membrane liquid 88
3. 2. 2. Creeping flow mode due to capillary action and buoyancy 90
3. 3. Emulsified liquid membranes (EML) 92
3. 3. 1. Mean drop diameters of *W/O*- and (*W/O*)/*W*-dispersion in an agitated vessel 92
3. 3. 2. Phase inversion in liquid-liquid dispersion 94
3. 3. 3. Breakage of EMLs 95
3. 3. 4. Effect of organic solvents on the stability of ELM 96
3. 3. 5. Water permeation coefficient and water entrainment in (*W/O*)/*W* dispersions 98
4. Separation of metal ions using supported liquid membranes 100
4. 1. Ion transport through an SLM containing crown ether 100
4. 2. Enrichment of cobalt in a multi hollow-fibers SLM module 104
4. 3. Fractional separation of metal ions in one-stage *CR*-SLM operation 104
4. 4. Recovery of Cr(VI) from sulfuric acid media using a flat-type SLM in continuous regeneration mode 107
5. Conclusion 109
6. References 110

1. Introduction

For devising new and highly-selective separation method by use of artificial membranes, it is crucial to model on the function of biological membranes. Biological membranes have a distinctive feature in the fast and selective transport, which can be grouped according to complexity into three categories: molecular diffusion; passive carrier transport; and active carrier transport.

The concept of a molecular carrier mechanism involving a reversible chemical combination between permeant and mobile species was developed by Osterhous *et al.*[1] in the early 1930s, using a weak organic acid as a carrier for sodium and potassium ions. Scholander (*1960*)[2] demonstrated a facilitated carrier-mediated transport that hemoglobin and myoglobin could accelerate the transfer of oxygen across water films. Furthermore, it was demonstrated that certain polypeptides (for example, valinomycin), cyclic polyethers, and polyether carboxylic acid (for example, monensin), could increase the transport of ions across lipid bilayer membranes by many orders of magnitude.

Much of the recent chemical engineering interest is to design and develop energy-saving processes due to the incorporation of specific chemical or biological reaction in separation systems. In liquid membrane separation, Ward and Robb (*1967*)[3] have suggested the separation of CO_2/O_2 by the facilitated transport through a supported liquid membrane (SLM). At 1968, on the other hand, the idea of emulsified liquid membrane (ELM) has been

proposed by Li.[4] Thereafter, a great number of investigations have been conducted on the two configurations of liquid membranes; however, only one process has been demonstrated in industrial scale at present.[5] This may be attributed for less stability of the membranes as thin bound film.

The present paper provides a review and discussion of our investigations on the membrane permeation and stabilities in both configurations of SLM and ELM, which are most significant in designing the processes for liquid membrane separation.

2. Permeation Rates across Liquid Membranes

In liquid membrane separation, the membrane transport can be broadly devided into three categories: carrier-mediated transport, where permeant, A, and carrier are in equilibrium with the reaction product (or their complex) in the membrane phase; carrier transport (or coupled transport), where only permeant-carrier complex diffuses across the membrane; and molecular diffusion with a reaction on the downstream side.

Permeation flux of A, J_A, is expressed by

$$J_A = [D_{Am}(\overline{C}_{AI} - \overline{C}_{AII})/\ell]\,(1 + F) \tag{1}$$

where D_{Am} is the diffusivity of A in the membrane phase, ℓ the diffusion-path length, $\overline{C}_A$ the concentration of A in the membrane, F the facilitation factor, and the subscript I and II refer to the two extremes of the membrane. In case of the coupled transport, F-value is zero since the permeant can not pass independently through the membrane, whereas both carrier-mediated transport and molecular diffusion with a reaction can be termed as the facilitated transport. Many analytical and approximate solutions for the facilitation factor have been reported, where the F-value increases with decreasing concentration of A and hence the separation factor is enchanced.

The situation of the coupled transport of a divalent metal cation M^{2+} through a liquid membrane is schematically illustrated in Fig. 2. 1, where the processes of interfacial chemical reactions occurring at the two extremes of the membrane, I and II, as well as the aqueous film diffusion and membrane diffusion are considered. To derive the flux equation describing the permeation across the membrane, the kinetics of the interfacial reaction should be taken into account together with the rate of diffusion through the aqueous boundary layers and membrane.

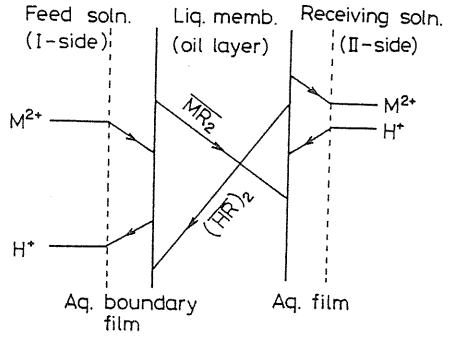

Fig. 2. 1. Schematic representation of concentration profiles of divalent metal ion (M^{2+}) for coupled transport across liquid membrane containing an extractant (HR).

2. 1. *Aqueous Film Mass-Transfer Coefficients*

The individual mass transfer coefficient for a liquid-liquid system can be determined

from the extraction experiments for two systems with different values of the distribution ratio, m, of solute. A simple method was proposed which enables the simultaneous determination of mass-transfer coefficients in both aqueous and oil phases from the single liquid-liquid extraction system.[6] The method is based on the measurements of extraction rates at two different concentrations of a solute having the value of m varying significantly with the concentration. This novel determination was demonstrated for an extraction system of water/iodine/toluene in a stirred vessel with flat interface.

An aqueous iodine solution contains the iodine species I_2, I^- and I_3^-:

$$I_2 + I^- \rightleftharpoons I_3^- \quad : \quad K_1 = 7.48 \times 10^2 \tag{2}$$

The distribution equilibrium of I_2 in n-heptane is expressed by

$$I_2 \rightleftharpoons \overline{I_2} \quad ; \quad K_2 = 36.6 \tag{3}$$

The equilibrium constant was determined from the distribution ratio given in Fig. 2. 2, where

$$m = [\overline{I_2}]/[I_2]^T = K_2/(1 + K_1[I^-]) \tag{4}$$

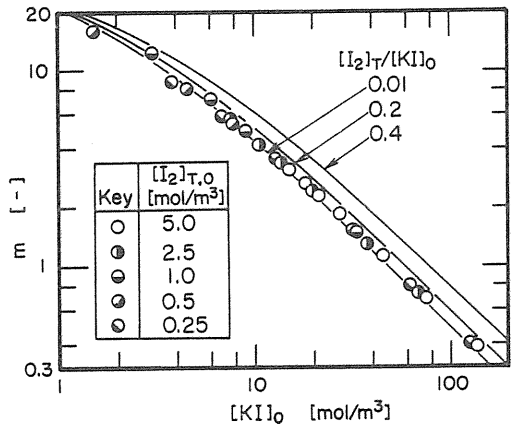

Fig. 2. 2. Distribution ratio of iodine between I_2-KI aqueous solution and *n*-heptane.

and the total concentration of iodine, $[I_2]^T = [I_2] + [I_3^-]$, determined by iodometry. In smaller $[I_2]^T/[KI]$, there is little effect of the concentration ratio on the value of m.

Aqueous phase mass-transfer coefficient was obtained in I_2 extraction through hydrophobic microporous membrane as a bound membrane wetted with an extractant solvent flowing on the recovery side. When a couple of the molar fluxes, J_1 and J_2, are observed for two aqueous feeds, *1* and *2*, with different concentrations of iodine at the same flow velocity, one can obtain the following relationships:

$$J_j = k_{wj}([I_2]_F^T - [I_2]_{Fi}^T)_{j,lm} = k_{mo}([\overline{I_2}]_i - [\overline{I_2}]_R)_{j,lm} \quad (5)$$

where subscript j represents *1* or *2* corresponding to the aqueous feed. The "apparent" organic-phase mass-transfer coefficient, k_{mo}, including the membrane phase, is assumed to be independent of the iodine concentration in the aqueous phase, $[KI]/[I_2]^T$.

Assuming that $k_{W1} = (D_1/D_2)^{2/3} k_{W2}$ in Eq. (5), one can obtain

$$k_{mo} = J_2/[\triangle C_2^* - (m_{2i}J_2/k_{W2})] \quad (6)$$

$$k_{W2} = J_1 J_2 \{m_{2i} - m_{1i}(D_2/D_1)^{2/3}/(J_1 \triangle C_2^* - J_2 \triangle C_1^*)\} \quad (7)$$

where $\triangle C_j^* = (m_i[\overline{I_2}]_F^T - [\overline{I_2}]_R)_{j,lm}$ (j=*1* or *2*) and m_i is at the aqueous-oil interface, D being the apparent diffusion coefficient of I_2 in the aqueous phase.[10] On the basis of the theoretical concept, the iodine extraction system was applied for determining aqueous film mass-transfer coefficient in two types of SLM modules: flat sheet and hollow-fiber modules.

2. 1. 1. Flat-Type Membrane Module[7]

A microporous flat membrane (MFM) was sandwiched with two spacers on which a channel of 3 mm width, 58 cm effective length and 1 mm (2, 3 or 5 mm) depth was prepared. The MFMs used were *Fluoropore* (*FP*) membrane (*Sumitomo Den-ko*) and *Duragard 2500* membrane (*Poly Plastic Co.*). The completed module was installed horizontally in an experimental apparatus, where an aqueous I_2-KI solution and *n*-heptane are supplied on the separate side of the module. The MFM in the device was impregnated with the extractant solvent by letting it soak out from the flowing side to the other side of the membrane. All the experimental runs were done at 25 ± 0.5°C. After attaining a steady state, liquid samples were taken from the influent and effluent streams. Iodine concentration was measured by iodometry for aqueous samples and by spectrophotometry at 522 *nm* for the *n*-heptane solution. The flux of I_2 extraction was then calculated in terms of the concentration difference of I_2 in the organic phases.

The values of k_w thus obtained are examined in terms of the dimensionless numbers of *Sh*, *Re* and *Sc* in general correlations. The values of *Sh* and *Re* were calculated based on the distance averaged in the flow direction, *X*, as the characteristic length; the results are plotted in Fig. 2. 3 as *Sh* vs. Re_X. It is to be noted that the *Re* dependence of *Sh* is 1/2 and there is no effect of the channel depth, *h*. The dashed line represents the theoretical equation of mass-transfer coefficient for fluid flows parallel to a flat plate, obtained by integrating a solution of the boundary-layer theory to flow direction.[8]

It was found that the present results are about 50% higher than for the flat solid plate. Such a difference may be attributed to the definition of fluid velocity, in which the velocity at an infinte point apart from the surface is adopted to the flat plate, whereas the mean value to the present membrane device with the narrow channel. When adopting the velocity duplicated the mean value, the difference in *Sh* between the solid plate and the present device is of no significance. Here, assuming the 2/3 power of *Sc* from previous theories on mass transfer and heat transfer, we find the following correlation

$$Sh_X = 1.0\ Re_X^{1/2}\ Sc^{1/3} \quad (8)$$

This equation is shown by solid line in Fig. 2. 3.

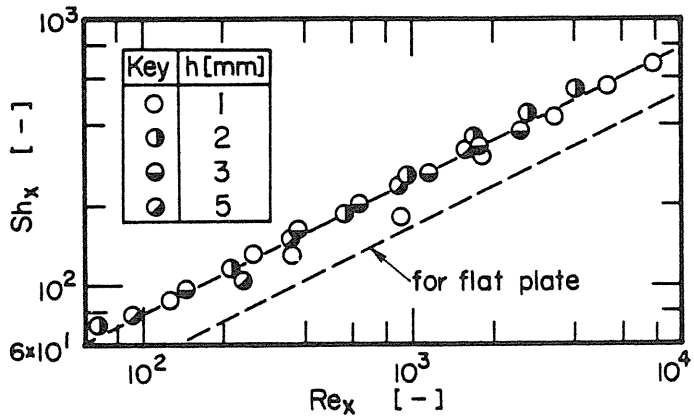

Fig. 2. 3. Correration of Sh_X with Re_X for iodine transport through aqueous boundary film on the oil-containing sheet membrane.

2. 1. 2. *Hollow-Fiber Module*[9)]

Microporous hollow fibers (MHFs) have been widely used in reverse osmosis (*RO*) modules and gas permeators or separators, because of their large surface per volume advantage. Most recently, the applicability of MHF contactors to equilibrium separation of aqueous solutions or gaseous mixtures is being explored in two operating modes-SLM and bound membrane. In the contactors, two fluid flows are almost completely independent; as a result, there is no constraint due to flooding, loading, or channeling. Furthermore, the bound membranes are free of constraints of membrane stability and its regeneration, hence offering an efficient liquid membrane extractor or absorber.

We carried out systematic measurements to obtain more accurate correlations of two liquid-phase mass-transfer coefficient, k_t and k_s, on the tube (lumen) and shell sides in single hydrophobic MHF contactors, adopting two contacting modes shown in Figs. 2. 4a and b. A diagram of an MHF module is shown in Fig. 2. 5. The module was designed to eliminate any entrance and exit effects. The MHFs used in this work were Teflon HFs (*GoreTex* tube of 50% porosity and 2 μm maximum pore diameter); the geometries are given in Table 2. 1

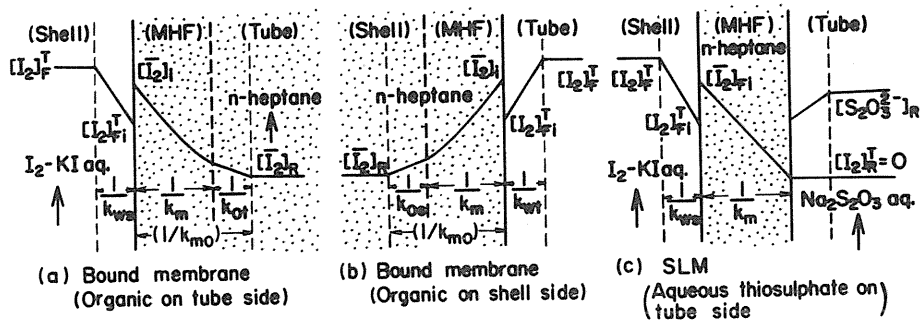

Fig. 2. 4. Plausible concentration profiles for hydrophobic MHF in three contacting modes.

together with the details of the modules used. An aqueous feed solution is supplied on the lumen side or shell side of the module installed horizontally in an experimental apparatus. An organic extractant (*n*-heptane) flowed on the module in once-through mode *via* the flow loop similar to the aqueous flow system. As the feed, we used two aqueous iodine solutions: $5.3\times10^{-3}M$ I_2 with $0.1M$ KI (feed *1*) and $6\times10^{-4}M$ I_2 with $4\times10^{-3}M$ KI (feed *2*).

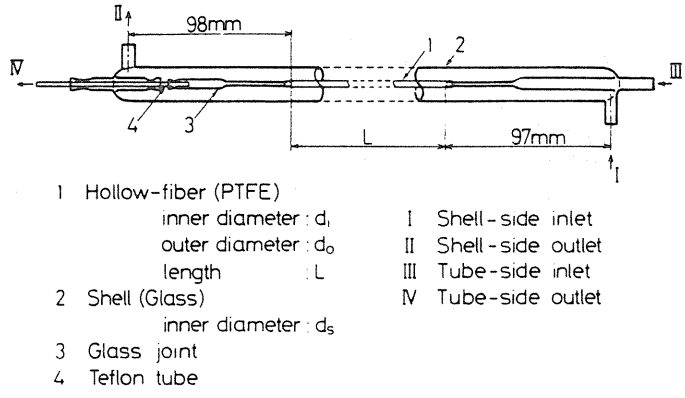

Fig. 2. 5. Diagram of the single MHF module.

Table 2. 1. Details of single HF modules. Symbols as in Fig. 2. 6.–8.

	module		hollow fiber (ϵ = 0.50)			
key	type	10^3d_s, m	type	10^3d_i, m	10^3d_o, m	10^3L, m
■	01LS	17.5	TA001	1.0	1.8	199
◧	01SS	7.6	TA001	1.0	1.8	199
○	02LS	17.5	TA002	2.0	2.8	194
◑	02SS	7.6	TA002	2.0	2.8	199
△	06LS	17.5	TA006	6.0	7.2	196
▲	06LM	17.5	TA006	6.0	7.2	294
▲	06LL	17.5	TA006	6.0	7.2	585
▽	12LS	17.5	TA012	12.0	14.0	202

Tube-Side Liquid Film Mass-Transfer Coefficient: The value of k_{wl} was determined from Eq. (5) for the aqueous feed on the tube side. The results are examined in terms of *Sh*, *Re* and *Sc*. Fig. 2. 6 shows a plot of *Sh* vs. *Re* based on the inner diameter of the MHF as the characteristic length. The solid lines represent Eq. (9), and the experimental results for $Re >$ 700 deviate remarkably from each line. This suggests that a transition from the laminar to the turbulent flow arose at about 700 ~ 800 in the *Re* range for the aqueous flow inside the oil-containing MHF, unlike fluid flow inside solid tube. Also, the effects of length and inner diameter of the MHF on *Sh* were represented by a relation of $Sh\,(d_i/L)^{-1/3}$. Here, assuming the 2/3 power of *Sc* in the same way as in deriving Eq. (8), we find the following correlation in the Graetz number range ($Gr \equiv (d_i/L)Re\cdot Sc$) of 50 ~ 1000:

$$k_t d_i/\mathrm{D} = 1.4\,(d_i/L)^{1/3}\,(d_i\,u_t/\nu)^{1/3}\,(\nu/D)^{1/3} \qquad (9)$$

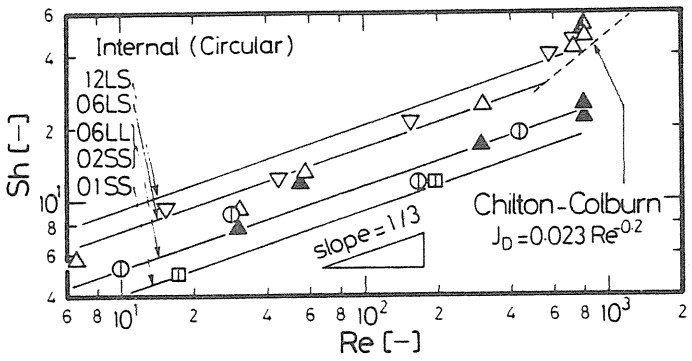

Fig. 2. 6. Effect of Reynolds number on Sherwood number for tube-side flow in MHF module.

This equation is lower by about 12% than result for gas absorption in a bound membrane contactor by Yang-Cussler[11] as well as that for a nonporous tube by Leveque.[12] In addition, Prasad-Sirkar[13] have reported that the k_t value in a hydrophobic MHF is smaller than that in a hydrophilic membrane. Such a difference may be due to the interfacial motion of a stagnant oil sublayer adhering on the surface of a hydrophobic MHF. This suggests that a nonslip condition for fluid flow at the interface is not valid to aqueous streamline flows over the oil-containing membranes.

Shell-Side Liquid Film Mass-Transfer Coefficient: The film mass-transfer coefficient, k_{ws}, for the aqueous flow on the shell side was obtained in the contacting mode shown in Fig. 2. 4b. The results were also examined in general dimensionless correlations. Here, we used a hydraulic equivalent diameter, d_e, difined as d_s-d_o, where d_s is the inner diameter of the shell tube, as the characteristic length in the annular space of the single MHF module.

The values of k_s are plotted against the shell-side fluid velocity in the dimensionless form in Fig. 2. 7, wherein solid line represents Eq. (10) in the lower *Re* region and Eq. (11)

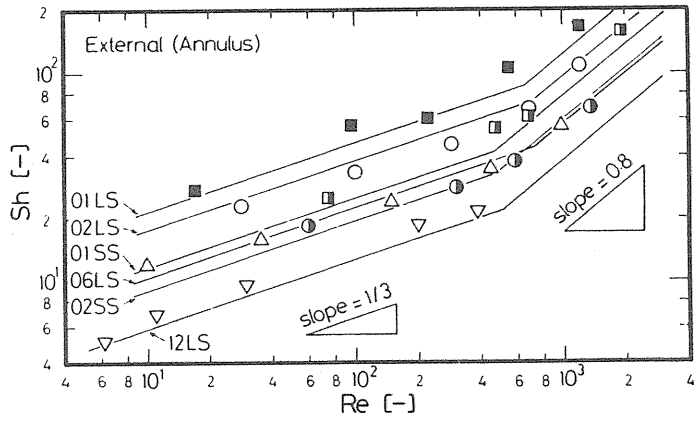

Fig. 2. 7. Effect of *Re* on *Sh* for annular flow on the shell side.

in the higher Re region. For laminar flow on the shell side, the 1/3 power of Re is found to be the same as that on the tube side, while for turbulent flow we assumed the exponent 0.8 from the Chilton and Colburn analogy.[14] In addition, it was found that the Sh varies with the 1/4 power of the tube length, L. With the exponent of 1/3 on Sc, the following equation can be derived for laminar flow in the annular space:

$$Sh = 0.85(d_s/d_o)^{0.45}(d_e/L)^{1/4}Re^{1/3}Sc^{1/3} \tag{10}$$

For turbulent flow, on the other hand, the effect of L on k_{ws} may be ignored in the same way as that for the usual flows inside a tube. The dependence of Sh on the diameter ratio, d_s/d_o, was found to be 0.57 on the basis of $Sh_{C\text{-}C}$ from the Chilton-Colburn equation for tube-side flow. The present results deviate from their equation with an increase in d_s/d_o; then the film transfer coefficient can be expressed by changing the constant, 0.023, into $0.017(d_s/d_o)^{0.57}$:

$$Sh = 0.017(d_s/d_o)^{0.57}Re^{0.80}Sc^{1/3} \tag{11}$$

Here, we attempted a comparison between the results obtained for the single MHF modules and previous correlations for multiple MHF extractors.[13,15] Though being significantly different from that in the single module, the shell-side flow in multiple MHFs modules should approach annular flow under a limiting condition. Fig. 2. 8 shows the comparison of the values of k_s in the single and multiple MHF modules, in terms of two parameters, d_e/L and d_s/d_o.

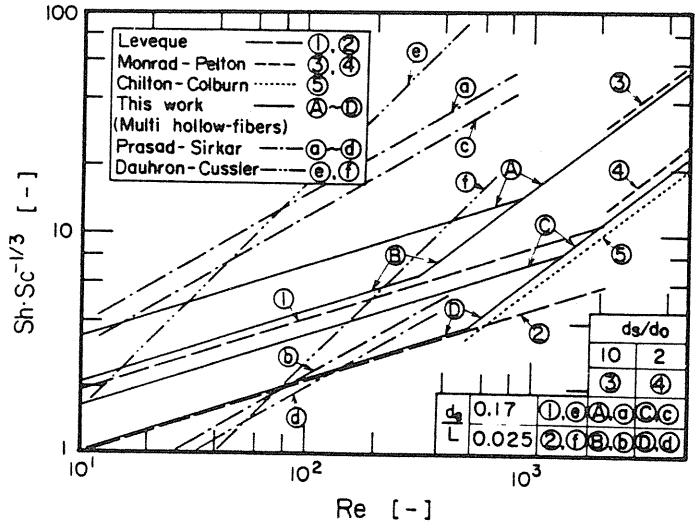

Fig. 2. 8. Comparison of shell-side mass-transfer coefficients in a single MHF with those for multiple MHFs.

The multiple MHFs have more significant effects of d_e/L and Re on k_s, as compared with single HF, having no calming section on the shell side; hence, it is considered that the velocity profile of the shell-side fluid was not fully developed in the devices having a short length. This indicates the possibility of a d_e/L overdependence of k_s. For the single MHF, it is noticed that Eq. (10) tends to converge to the Leveque solution as both values of d_e/L and d_s/d_o become smaller. Such a behavior suggests that there is no substantial difference in the aqueous-film transfer coefficients on the two sides of the HF.

2. 2. *Membrane-Transfer Coefficient*

To evaluate the permeation rate of A-species across an SLM, it is necessary to know the value of inherent diffusivity, D_{Am}, of the permeant in heterogeneous media (fluid-filled pores of the porous solid) and the diffusion path-length, ℓ, as well as the effective area for the permeation: $k_m = D_{Am}\,\varepsilon/\ell$.

2. 2. 1. *Effective Diffusivity*[7,9,17]

Membrane mass-transfer coefficient was determined in both operations of the bound-type membrane and SLM. In the former the total resistance in I_2 transport through the oil phase, $1/k_{mo}$, could be expressed as the sum of two resistances of the membrane layer, $1/k_m$, and the oil boundary film, $1/k_o$. When the organic liquid flowed on the tube side, one obtains

$$1/k_m\,d_{lm} = 1/k_{mo}\,d_o - 1/k_{ot}\,d_i \tag{12}$$

In the SLM operation (Fig. 2. 4c), iodine is extracted from the aqueous feed into the membrane phase and diffuses through the SLM. If the receiving phase contained thiosulfate ion, then the iodine can be reduced at the oil-aqueous interface; thus, $[I_2]_{Ri}=0$. Obtaining the extraction rate of iodine, N, by the SLM, one can determine the membrane-transfer coefficient as

$$k_m = (N/A_m)/m_i\{[I_2]_F^T - (N/k_wA_{ex})\} \tag{13}$$

where $N = k_wA_{ex}([I_2] - [I_2]_{Fi}^T)$ and the m_i value is for $[I_2]_{Fi}^T$. For the MFM module, $A_m = A_{ex}$, while A_m for the MHF is the logarithmic mean area, A_{lm}, based on d_i and d_o. This k_m-determination becomes simpler and more accurate than the bound-type membrane method, because of eliminating the diffusional resistance through aqueous boundary film on the recovery side by utilizing the redox reaction.

Fig. 2. 9a illustrates the effect of pore size, d_p, of FP-membrane on k_m and k_{mo}, indicating that the diffusional resistance through the oil-containing membrane is predominant. Furthermore, the results of k_m are also plotted in Fig. 2. 9 as $k_m/(D\varepsilon/\delta)$ versus d_p, where we used D=3.42×10^{-9} m^2/s as the diffusion coefficient of I_2 in n-heptane together with ε and δ in Table 2. 2. The value of $D\varepsilon/\delta$ is a theoretical membrane-transfer coefficient across a homogeneous oil layer of δ in thickness, and hence the ordinate of Fig. 2. 9a represents the reciprocal of tortuosity of the MFM, $1/\tau$, being then in the range of 0.2 to 0.3. In the case of Duragard membrane, however, the value of $1/\tau$ was found to be 0.14.

On the other hand, the results obtained for the various MHFs (See Table 2. 1) are shown as a plot of $k_m/(D\varepsilon/\delta)$ against d_i/d_o in Fig. 2. 9b. It is evident that the value of k_m depends not only on the geometry of the HF but also the operating mode. If the MHFs used in the present experiment had uniform pore structure, the value of k_m or τ should be

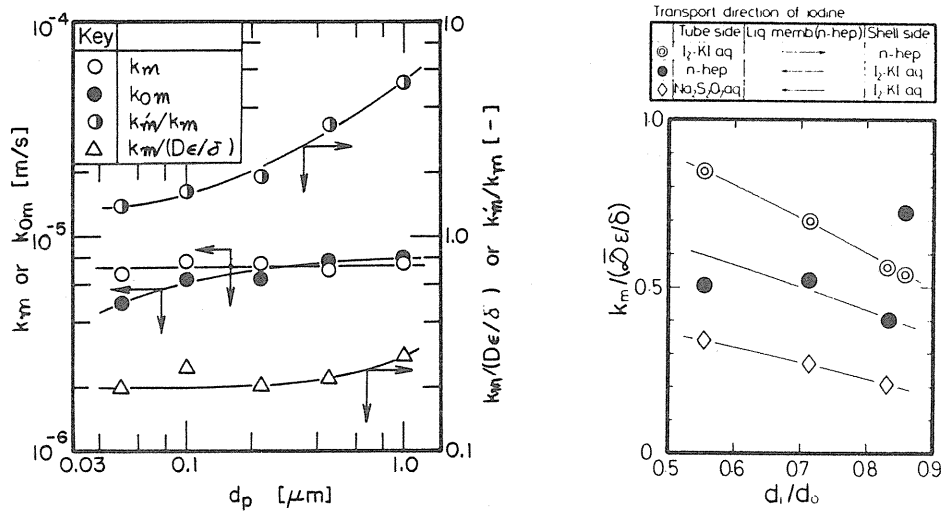

Fig. 2. 9. Variation of membrane-transfer coefficients through oil-containing membranes. a) Effect of pore size on k_m, k_{om}, $k_m/(D\varepsilon/\delta)$ or k'_m/k_m for the sheet membranes. b) Effect of the diameter ratio for MHFs.

Table 2. 2. Thickness, pore size and porosity of microporous *FP*-membranes.

Porous membrane	δ [μm]	d_p [μm]	ε[%]
FP−005	45	0.05	45
FP−010	60	0.10	55
FP−022	60	0.22	65
FP−045	80	0.45	75
FP−100	100	1.0	80
DG2500	25	0.4×0.04	45

* from manufacture's catalogue

independent of d_i/d_o as well as the direction of the solute transfer through the liquid membrane layer. Thus, it is to be expected that *GoreTex HF* is not uniform in the porosity profile through the wall thickness.

Diffusion in porous media effectively takes place over a larger distance than it would be in homogeneous media. To account for the reduced area of longer pores, the concept of effective diffusivity is available; $D_e=D_m/\tau$, and τ is the tortuosity to be between 2 and 6, averaging about 3. In periodic composite, D_e can be calculated exactly by $D_e/D_m=2(1-\phi_s)/(2-\phi_s)$,[16] where ϕ_s is the volume fraction of the solid sphere in the composite. When $\phi_s=(1-\varepsilon)=0.5$, we can obtain $D_e/D_m=2/5$.

Effect of the structural characteristics of solid support on the permeation flux through SLM was examined using various MHFs in a continuous regenerating mode, which will be

described in *3. 2. 2.* Fig. 2. 10 shows the effects of ε and d_p on the value of D_e obtained for a Ni-(HDEHP/n-heptane) system, indicating that D_e depends on $\varepsilon^2 d_p^{1/2}$. Such a structure dependence may be due to the surface free area of the solid support.[17] According to Pons, [18] the fraction of surface free area, ξ, for *Millipore* and *Gore-Tex* membranes is in direct proportion to $\varepsilon^{2.118}$ in the ε-range of 0.5 to 0.9, and also the hydraulic radius of the pores is in direct proportion to $d_p^{1/2}$. Good agreement in the structure dependence of D_e and ξ is probably due to a "*surface effect*" that was lumped together in calculating the permeation flux across the SLM.

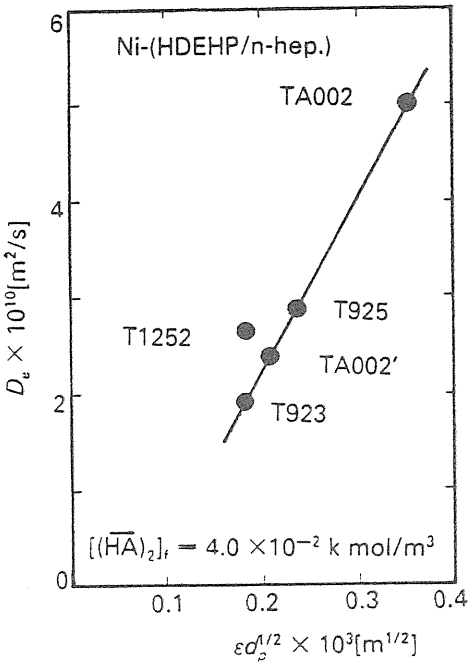

Fig. 2. 10. Correlation of effective diffusivity with the pore size and porosity of MHFs.

2. 2. 2. *Effective Diffusional Length and Interfacial Area.*[19–21]

In the situation of mass transport across an SLM, it is not very easy to obtain the accurate value of k_m. We examined the area effective to the contact between ester phase and *Millipore filter* (*NR*) filled with an aqueous NaOH solution, using a bound-type diaphragm cell.[20] The results for the hydrolysis of various esters were interpreted on the basis of mass transfer with a pseudo first-order chemical reaction, and the effective interfacial area, a_e, obtained for the liquid-liquid membrane contacting systems is plotted in Fig. 2. 11 against the interfacial tension, γ.

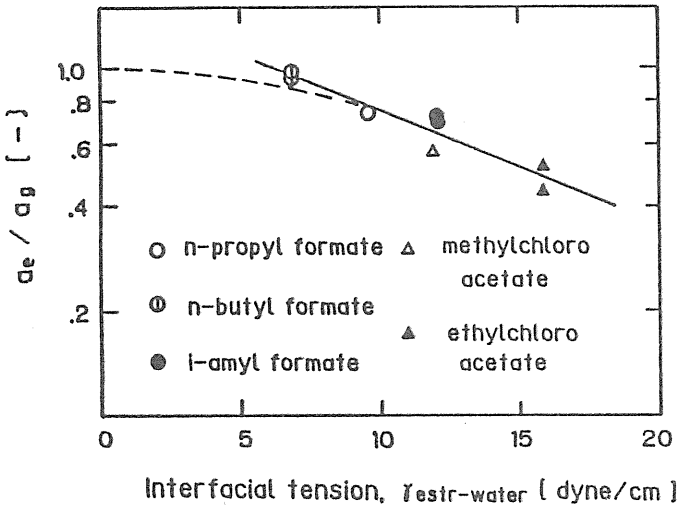

Fig. 2. 11. Effect of interfacial tension on the effective area for hydrolysis of various esters.

In the a-determination, we assumed that the diffusion path-length, ℓ, across the membrane layer has a constant value. In other words, when considering that the geometric area, a_g, of the filter ($\pi d_p^2 \varepsilon/4$) is identical with the interface between the ester and aqueous phases, the value of ℓ should vary with the interfacial tension, depending on the kind of the esters. This suggests that a thin stagnant layer of the membrane liquid is formed on the filter surface and then its thickness varies with the physico-chemical and thermodynamic properties such as kinematic viscosity, ν, and γ as well as the hydrophobicity of solid support.

Fig. 2. 12 represents the effect of ν on the values of ℓ for gas- and liquid-liquid membrane systems with various kinds of *Millipore* filters in a diaphragm cell.[5] In the case of Teflon filter (LS), the ℓ-value for the membrane filled with aqueous solution is independent of ν, being only 30% higher than the filter thickness, δ, while that with an organic solution by a factor of 3: $\ell \simeq 3\delta$. For hydrophilic or less hydrophobic filters, on the other

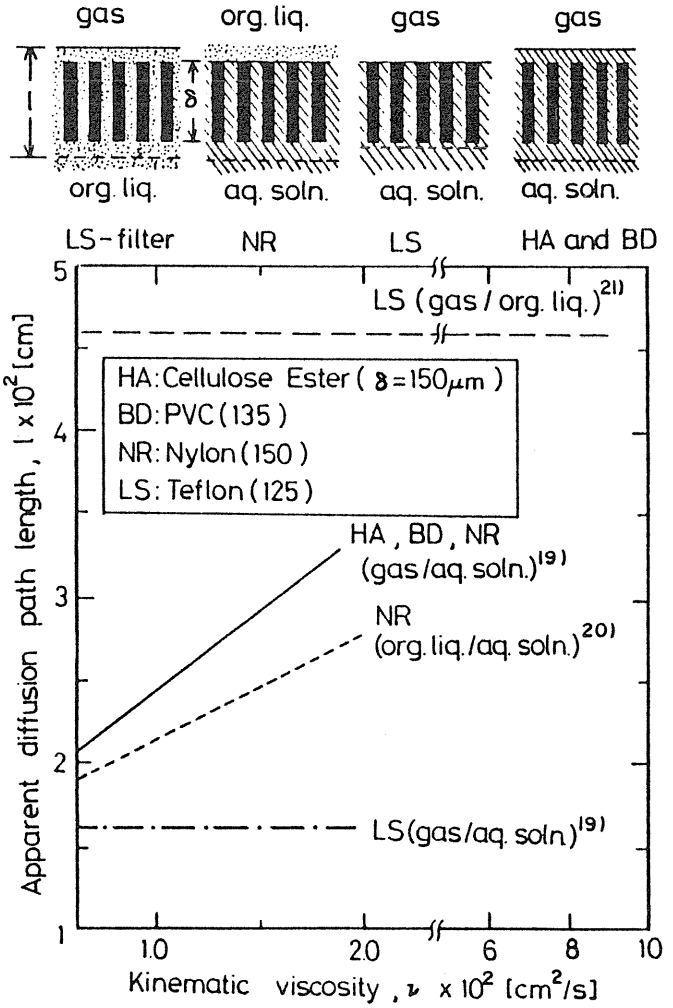

Fig. 2. 12. Apparent, diffusional-path length for various SLM systems of Millipore filters.

hand, the ℓ-values increased with an increase in v. This leads to a uncertainty in the path length for solute diffusion across the oil-containing membrane. Also, the pore entrance and exit effects might become more significant with an increase in the thickness of the stagnant sublayer, as suggested by Malon and Anderson.[23] When flowing together with aqueous feed or recovery solution in an SLM operation, the membrane oil could renew the stagnant layer, being partly interchanged with the membrane phase. This causes an apparent enhancement of k_m for SLM as shown by k'_m/k_m in Fig. 2. 9a.

From this discussion, a conclusion can be drawn that the application of τ to the oil-containing membrane is limited. No further discussion of the membrane-transfer coefficient will be made here, since there is no reliable evidence that aqueous-oil interface was just on the surface of the microporous solid support.

2. 3. *Interfacial Chemical Reaction*

For some solvent-extraction systems, the kinetics were examined on the basis of the extraction and stripping rates through stirred plane interface or the surface of dispersed drops.

2. 3. 1. *Extraction of Copper by LIX65N*[24–29]

A commercial extractant LIX65*N* is β-hydroxy benzophenene oxime, extracting copper from dilute acidic leach liquors due to the formation of an extractable chelate-complex. Also in solvent extraction accompanied by such a chelating reaction, the extraction rate is controlled both by the kinetics of the reaction and by the diffusional characteristics of the system. Thus, studies were made on the extraction of Cu(II) from aqueous solutions by LIX65*N* in liquid-liquid dispersions under stirred conditions.

Equilibrium Distribution of Copper, m: The equilibrium distributions of copper between the organic and aqueous phases were determined on the basis of the concentration in the aqueous phase, C_w. In the case of very small change in C_w, the organic phase was also analyzed. Typical results of $m(=C_o/C_w)$ for the 10 vol% LIX65*N* system are shown in Fig. 2. 13 as a plot of m vs. C_w. The values of m become constant as C_w or pH decreases, then for the dilute acid solution being not dependent upon C_w. For $pH>3$ and $C_w>5\times10^{-4}M$, no appreciable effect of pH on m was found. Such behavior is due to the depletion of the active component of LIX65*N* by a reaction with the copper; then, the m-value varies in inverse proportion to C_w. For the lower C_w, however, its value varied as the square of pH.

Forward Extraction Rate N_f: A stirred vessel was used for the batch-wise extraction, which consisted of acrylic resin tube of 10 cm *i.d.* and 15 cm length fitted with four baffles and water jacket. The stirrer for liquid-liquid dispersion comprised two impellers with six-bladed turbine set at 2.5 and 7.5 cm from the bottom of the vessel. Aqueous solutions as the continuous phase were of copper sulfate ($C_{WO}=10^{-3}\sim10^{-2}M$); the dispersed phase was the kerosene solutions of LIX65*N* (2.5 and 10 vol%); the fractional dispersed organic volume was 10% and the temperature was controlled at 25 ± 0.5°C.

In the extraction runs, samples of about 3 *ml* were taken from the vessel at 30 sec intervals; the Cu concentration and pH value in the aqueous phase were measured on an atomic absorption spectrophotometer and a pH-meter, respectively. On the other hand, in the backward extraction runs, the copper dissolved in the dispersed organic phase was back-extracted by a sulfuric acid solution.

The extraction mechanism for Cu(II) with LIX65*N* is expressed by an overall reaction:

$$Cu^{2+} + 2RH \rightarrow CuR_2 + 2H^+ \qquad (14)$$

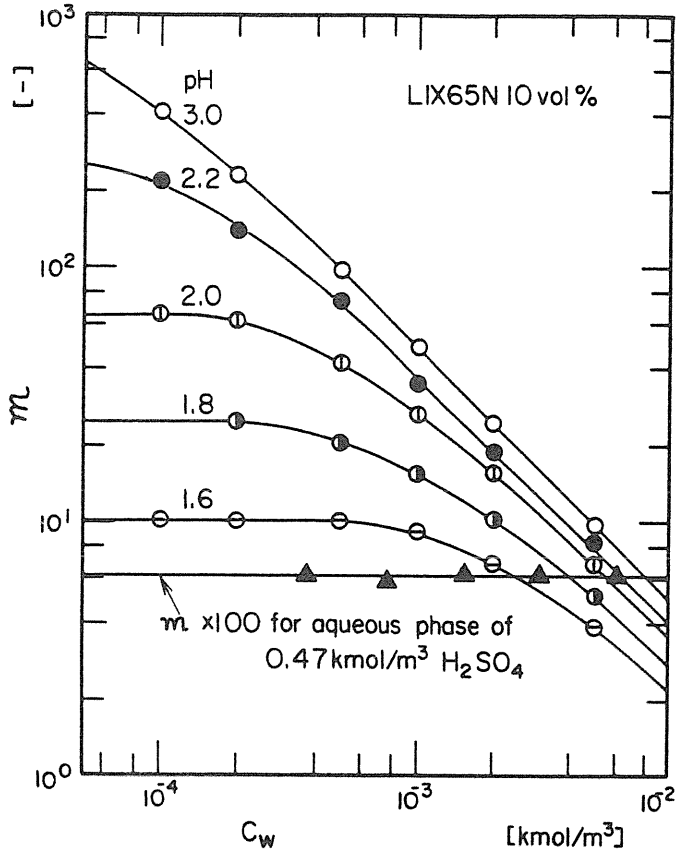

Fig. 2. 13. Plot of distribution ratio of Cu(II) against the aqueous concentration.

where RH is the active component of LIX65N. The rate of Cu(II) extraction, N_f, was evaluated from the time-dependent change in C_w by using the interfacial area, a, calculated from the Sauter mean diameter of dispersed drops, d_{32}, together with the fractional volume of dispersed phase, ϕ_o, given in Table 2. 3. Also both interfacial concentrations of RH and C_W

Table 2. 3. Sauter mean diameters of dispersed drops and mass-transfer coefficients in aqueous and organic phases.

LIX65N [vol%]	n [rpm]	$d_{32} \times 10^4$ [m]	$k_W \times 10^5$ [m/s]	$k_O \times 10^5$ [m/s]
10	300	5.52	1.00	0.64
10	400	3.20	1.26	1.10
10	500	2.09	1.50	1.69
10	600	1.48	1.71	2.38
5	500	2.22	1.50	1.59
2.5	500	2.60	1.50	1.36

were evaluated on the basis of mass-transfer coefficient for each phase, k_O and k_W. Fig. 2. 14 shows a plot of N_f vs. $[Cu^{2+}]_i\,[\overline{RH}]_i/a_H^+$, whereby the extraction rates are best fitted by

$$N_f = 8.19 \times 10^{-8}\,[Cu^{2+}\,[\overline{RH}]/a_H^+ \tag{15}$$

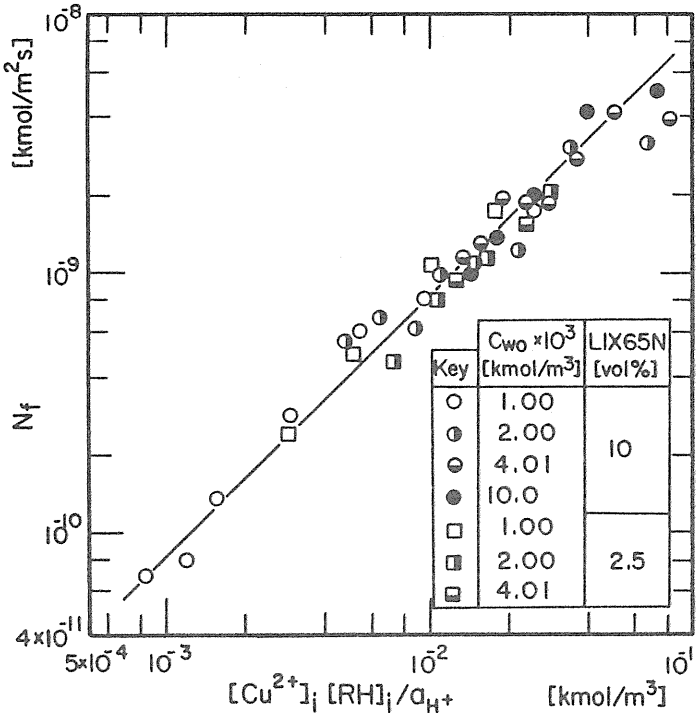

Fig. 2. 14. Correlation of the rates of forward extraction rates of Cu(II).

Backward Extraction Rate, N_b: Rate of the backward extraction is to be equal to the forward one under equilibrium conditions. Therefore, it is possible to evaluate N_b from Eq. (15) with the equilibrium data. Fig. 2. 15 shows a plot of the values of N_b thus obtained against $[CuR_2]a_H^+$, together with the N_b observed in the back-extraction runs, indicating that both of the calculated and the experimental values are correlated with a single straight line. A conclusion can be drawn that the overall-reaction rate R_o for the Cu(II) extraction by LIX65*N*-kerosene solutions is expressed by

$$\begin{aligned} R_O = N_f - N_b &= 8.19 \times 10^{-8}\,([Cu^{2+}]\,[\overline{RH}]/a_H^+) \\ &\quad - 3.63 \times 10^{-7}\,[\overline{CuR_2}]a_H^+ \end{aligned} \tag{16}$$

Here, considering a change in the interfacial tension, we attempted to estimate the copper-complex concentration at the liquid-liquid interface; then, we obtained the reaction

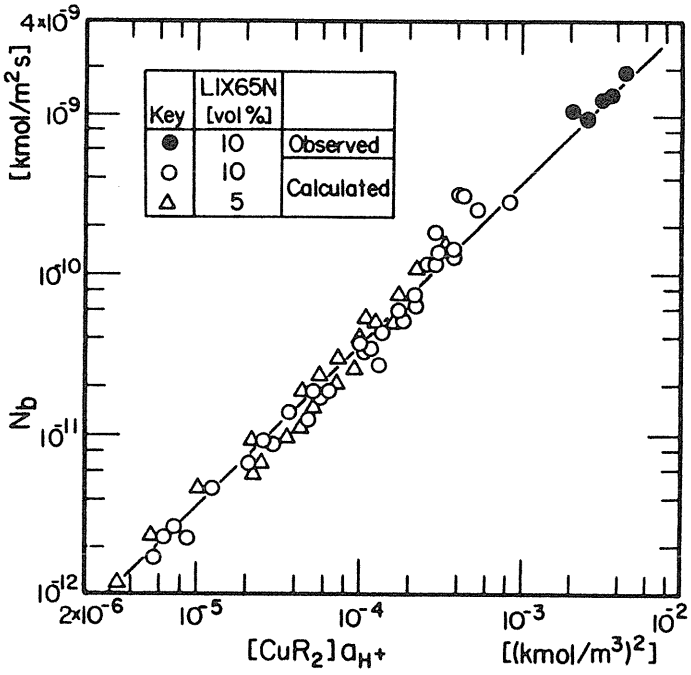

Fig. 2. 15. Correlation of the backward extraction rates of copper.

rate as

$$R_f = 6.9 \times 10^{-8} [Cu^2]_i^{0.85} ([\overline{RH}]_i/[H^+]_i)^{1.4} \tag{17}$$

Also, the stripping reaction rate for $[H^+] > 0.3M$ was given by

$$R_b = 2.5 \times 10^{-8} [\overline{CuR_2}]_i^{0.85} [H^+]^{0.7} \tag{18}$$

An increase in the interfacial tension with the copper concentration in the organic phase is caused with increasing acid concentration in the aqueous phase; however, the copper complex adsorbed at the interface may be in equilibrium with the aqueous phase. This suggests that there are two resistances to the copper stripping at the interface: the resistance to adsorption of Cu-complexes from the oil phase onto the interface, and that to the reaction between the adsorbed Cu-complexes and hydrogen ion in the aqueous phase.

2. 3. 2. *Extraction of Chromium* (VI) *by 3-(4-Pyridyl)-1,5-Diphenyl Pentane*[30]

The solvent extraction of Cr(VI) from aqueous solutions of H_2SO_4 with *3-(4-*pyridyl)-*1,5-*diphenyl pentane (*PDPP* or *B*) in nitrobenzene was studied at 25°C. The extracting reagent has a nature similar to tertiary amines, also being insoluble to water. However, the solubilites of Cr(VI)-*PDPP* complexes in aliphatic solvents are low, and a third phase is liable to form in the organic phase. In this section, the extractable ionic species of Cr(VI) is discussed

in terms of the dependence of m on the pH value and Cr(VI) concentration in aqueous phase. The interfacial reaction rate is evaluated from the extraction and stripping rates in a laminar liquid-liquid jet as well as a stirred vessel with a plane interface.

Distribution Equilibrium of Cr(VI): The distribution ratio of Cr(VI), $m(=[\overline{Cr}/[Cr])$, was determined between aqueous solutions of $K_2Cr_2O_7$(C_W=[Cr]=0.002 ~ 0.2M, pH0.6 ~ 5) and nitrobenzene solutions of *PDPP* ($[\overline{B}]$=0.025 ~ 0.63M). Typical results obtained at the initial concentration of Cr(VI) of 0.01M are plotted in Fig. 2. 16 as a plot of log m vs pH.

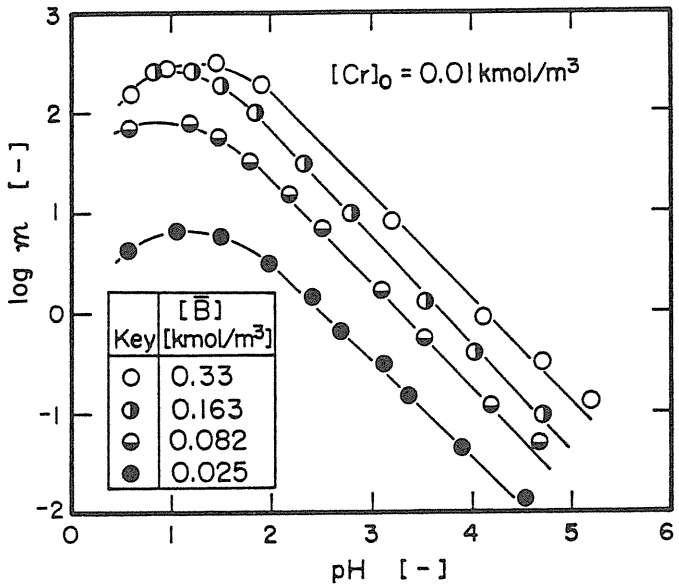

Fig. 2. 16. Effect of extractant (*PDPP*) concentration on the distribution ratio of Cr(VI).

The maximum loading ratio of Cr(VI) to *PDPP*, which was attained at $pH \simeq 1$ in an excess amount of Cr(VI), was between 1.2 and 1.4, but it increased slightly with $[B]$. In the present extraction system, sulfuric acid can also be extracted by *PDPP*; however, both of Cr(VI) and H_2SO_4 were extracted independently at pH2, while the two species competed with each other in the extraction at lower pH.

Hexavalent chromium in aqueous solution exhibits multi-equilibria among the various ionic species; these concentrations in the acid solution can be determined from the mass balance equations using the relevant equilibrium constants. The calculation results are shown in Fig. 2. 17 as the concentration ratios to [Cr], indicating that the dominant species of Cr(VI) are $Cr_2O_7^{2-}$ and $HCrO_4^-$ for $pH > 2$. Thus the equilibrium data of Cr(VI) distribution were examined in terms of the two ions. It was found that Cr(VI) in the aqueous phase is extracted into the organic phase with *PDPP* through the reaction:

$$HCrO_4^- + H^+ + \overline{nB} \leftrightarrows \overline{B_nH_2CrO_4} \qquad (19)$$

On the basis of the dependence of m on $[\overline{B}]$, shown in Fig. 2. 16, the distribution

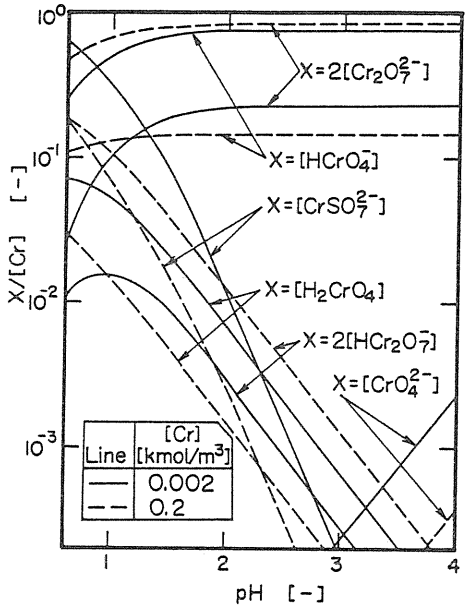

Fig. 2. 17. Fraction of each ionic species of Cr(VI) in the aqueous phase.

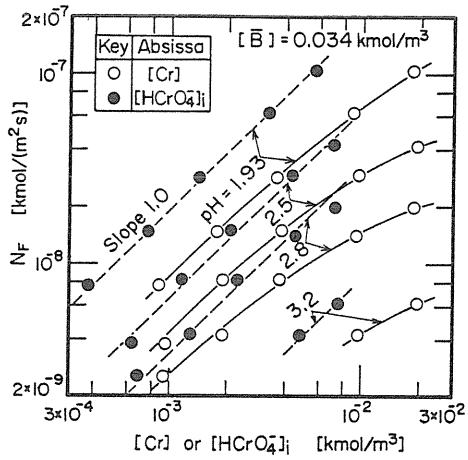

Fig. 2. 18. Rate of Cr(VI) extraction obtained in stirred vessel with a plane interface.

equilibria for the loading ratio of $[\overline{Cr}]/[\overline{B}] < 0.5$ are expressed by

$$[\overline{Cr}] = 1.5 \times 10^5 \, [HCrO_4][H^+][\overline{B}]^{1.5} \tag{20}$$

Rate of Cr(VI) *Extraction*: The results for the extraction of Cr(VI) are shown in Figs. 2. 18 and 19, where the interfacial concentrations of $[HCrO_4^-]_i$ and $[H^+]_i$ were calculated on the basis of the mass transfer of Cr(VI) and H^+ through the aqueous boundary film. Fig. 2. 18 shows that the value of N_f is proportional to $[HCrO_4]_i$, as illustrated by the dashed line. In Fig. 2. 19, $N_f/[HCrO_4^-]_i$ increases in proportion to $[H^+]_i$.

On the other hand, the rate of the backward extraction, N_b, is proportional to $[\overline{Cr}]_i$ as shown in Fig. 2. 20. The overall extraction rate or stripping rate can be expressed as a difference between the forward reaction rate, R_f, and the backward one, R_b. Neglecting the effect of R_f on R_b in the *pH* range of 4 to 9, we obtained the backward reaction rate from the results of N_b as

$$R_b = 9 \times 10^{-7} \, [\overline{Cr}]_i \, [\overline{B}]^{-0.5} \tag{21}$$

The R_f value calculated as $(N_f + R_b)$ is given in Fig. 2. 19. Furthermore, being equal to R_b under the equilibrium conditions, R_f can be derived from Eq. (21) as follows:

$$R_f = 0.135\ [H^+]_i\ [HCrO_4^-]_i\ [\bar{B}] \tag{22}$$

This rate equation is shown by the dashed line in Fig. 2. 19. The experimental values of R_f for $[H^+] < 10^{-2}$ M are in good agreement with Eq. (22) except for the large $[\bar{B}]$.

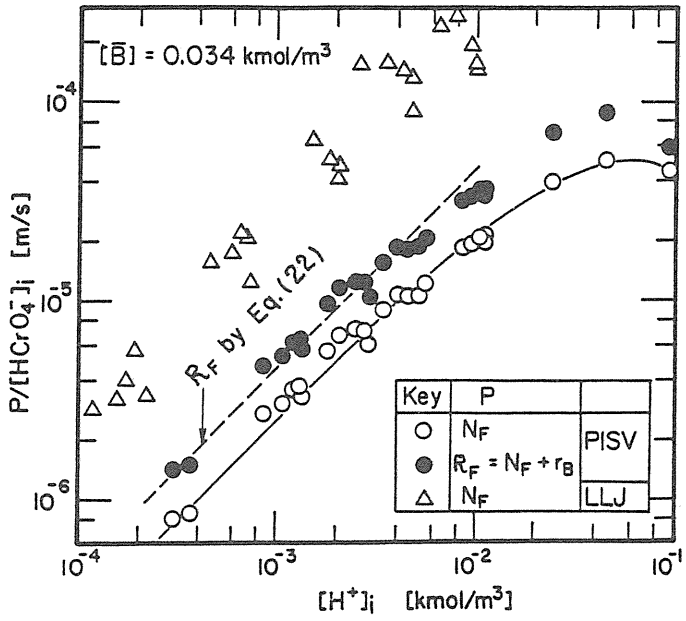

Fig. 2. 19. Effect of $[H^+]_i$ on the extraction rate and forward reaction rate for Cr(VI).

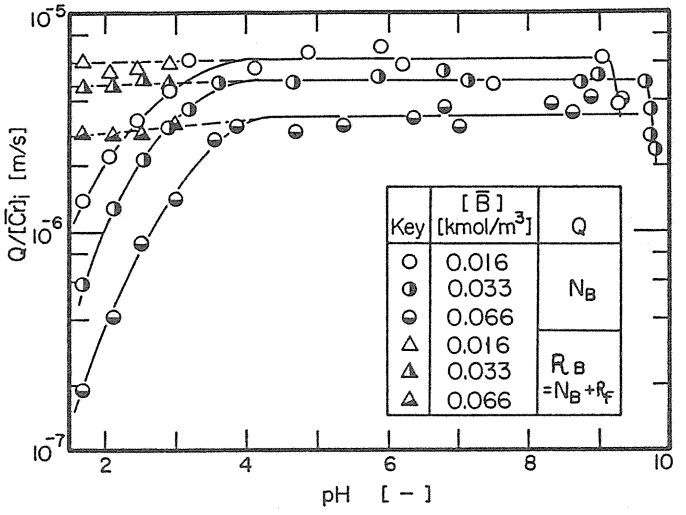

Fig. 2. 20. Effect of *pH* on the stripping rate and backward reaction rate for Cr(VI).

2. 3. 3. *Extraction Equilibria of Di- and Tri-Valent Metal Ions by 2-Ethylhexyl Phosphonic Acid Mono-(2-Ethylhexyl) Ester*[31]

When considering the liquid membrane separation of valuable metal ions in aqueous solutions, it is necessary to know not only the equilibrium distribution of its ion but also the extracted species of interest in the lower concentration range of H^+, compared to the solvent extraction. Nevertheless, even in the extensive data on the typical extraction system of di-(2-ethyl hexyl) phosphoric acid (D2EHPA)-lantanides and/or actinides, this area has received relatively little study to date, from the difficulties encountered due to gel formation at low acidities and moderate lantanides concentrations.

In this section, studies were made on the extraction of La(III) typical of all trivalent rare earth metals and Cu(II) and Co(II) of divalent heavy metals into *n*-heptane solutions of *PC-88A* as an organophosphorous extractant from weak acid media in the *pH* range of 2 ~ 5. The extractant reagent had a purity of 95%, being diluted with *n*-heptane to a given content (1, 2, 5, 7, 10, and 20 vol% of *PC-88A*) without further purification. Aqueous solutions of $LaCl_3 \cdot 7H_2O$, $CuSO_4 \cdot 5H_2O$ and $CoSO_4 \cdot 7H_2O$ of analytical grade were used and each solution *pH* was adjusted with diluted HCl (or H_2SO_4) or CH_3COOH/CH_3COONa buffer at a constant ionic strength. The equilibrium concentrations of La in both aqueous and organic back-extracting phases were determined spectrophotometrically with 0.1% Arsenazo III.

$LaCl_3$-(PC-88A) System: According to Tanaka,[32] the extraction equilibria of metalic ion M^{n+} by non-chelating reagent *HR* can be expressed as

$$jM^{n+} + \frac{r}{2}(\overline{HR})_2 \leftrightarrows (\overline{M_jR_rH_h}) + n_j\,H^+ \tag{23}$$

where $nj+h=r$. By defining

$$K_{ex} = [\overline{M_jR_rH_h}][H^+]^{nj}/[M^{n+}]^j[(\overline{HR})_2]^{r/2} \tag{24}$$

and assuming only *j*-polymeric extracted species in organic phase, its concentration can be expressed as

$$\log C_o = j(\log C_w - n \cdot \log[H^+]) + \log K_{ex} - \log[(\overline{HR})_2]^{r/2} \tag{25}$$

where $C_o=j[\overline{M_jR_rH_h}]$ and $C_w=[M^{n+}]$. Therefore, the slope of the line for a ($\log C_o$) *vs.* ($\log C_w - n \cdot \log[H^+]$) plot at a constant $[(\overline{HR})_2]$ represents the degree of polymerization, *j*. A semi-log plot of $m(=C_o/C_w)$ *vs. pH* gives a slope of 3 at a fixed *PC-88A* concentration, which indicates a molar ratio of 1:3 for the reaction between La^{3+} and *PC-88A* in Eq. (23): $n=3$. Fig. 2. 21 represents the log-log plot corresponding to Eq. (25), suggesting that $j=1$ and $r=6$, *viz.*, the formula of the extracted species in *n*-heptane is $LaR_3 \cdot 3HR$. From the above discussion, we may conclude that the reaction for this extraction system takes place according to the following equation:

$$La^{3+} + 3(\overline{HR})_2 \leftrightarrows \overline{LaR_3 \cdot 3HR} + 3H^+ \tag{26}$$

Such an ion-exchange mechanism for the extraction of lanthanum from weak acid media with *PC-88A* corresponds to the results for the extraction of lantanides at a tracer concentration by D2EHPA.

$CuSO_4$- and $CoSO_4$-(PC-88A) Systems: Typical results obtained for the present systems are shown in Figs. 2. 22a and b together with the data for the binary cation system. In the extraction of Cu(II), the pH-dependencies of m gradually decrease from 2 to 1 less with increasing solution pH in the range of $2 \sim 5$, whereas for the Co(II) system the slope of the lines is 2. The reaction between Cu(II) or Co(II) and *PC-88A* can also be determined by the same method as used for the lanthanum system. Then we found that the formula of extracted species is $CuR_2 \cdot 2HR$ and $CoR_2 \cdot 2HR$; the extraction equilibria can be expressed as

$$M^{2+} + 2(\overline{HR})_2 \leftrightarrows \overline{MR_2 \cdot 2HR} + 2H^+ \tag{27}$$

where M^{2+} represents Cu^{2+} or Co^{2+}. In addition, it was found that at the concentrations of $10^{-4} \sim 10^{-5} M$, there is no appreciable difference between the single and the binary systems of Cu(II) and Co(II).

2. 3. 4. *Extraction of Cadmium* (II) *by D2EHPA*[33,34]

Solvent effect on the Cd(II) extraction by D2EHPA was examined for four organic solutions of *n*-heptane, kerosene, toluene and *m*-xylene. Each solvent had the same *pH*-dependence of m as found for the Co(II)-D2EHPA/*n*-heptane system mentioned above; then, the extractability had the highest value in aliphatic hydrocarbons and lowered in the following sequence:

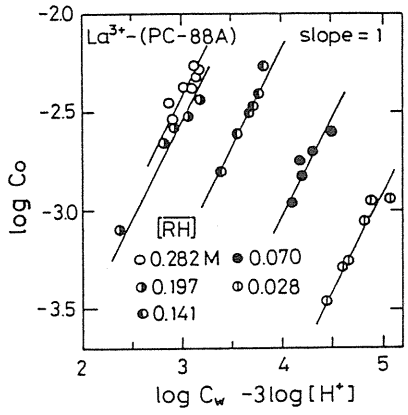

Fig. 2. 21. Plot of log C_0 versus (log C_W − 3 log $[H^+]$) for La^{3+}-(PC-88A/*n*-heptane) system.

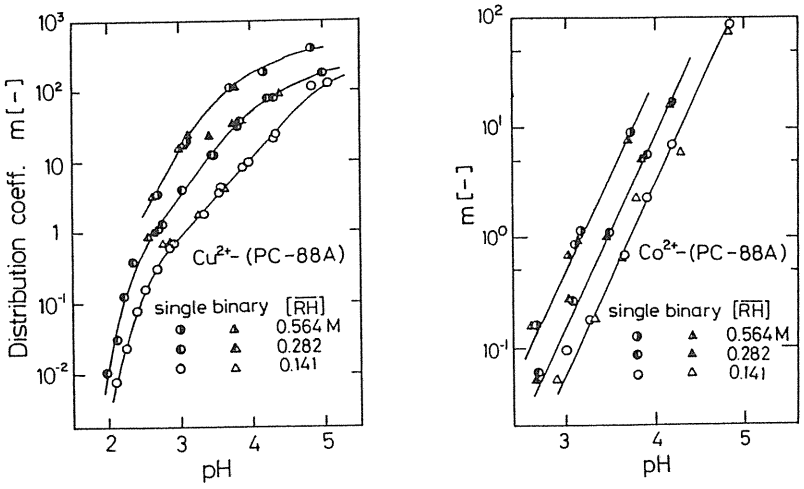

Fig. 2. 22. Plot of distribution ratio versus solution *pH*.
a) Cu(II)-(PC-88A/*n*-heptane) system with and without Co(II).
b) Co(II)-(PC-88A/*n*-heptane) system with and without Cu(II).

n-heptane > kerosene > *m*-xylene > toluene. The extracted species were determined on the basis of Eq. (25) as shown in Fig. 2. 23, wherein the value of (log[Cd]+2*pH*) is plotted against $[(\overline{HR})_2]$ at a constant $[\overline{Cd}]$. Then the extraction equilibria can be expressed by

$$Cd^{2+} + \frac{5}{2}(\overline{HR})_2 \leftrightarrows \overline{CdR_2 \cdot 3HR} + 2H^+ \quad : \text{(Aliphatics)} \tag{28}$$

$$Cd^{2+} + 3(\overline{HR})_2 \leftrightarrows \overline{CdR_2 \cdot 4HR} + 2H^+ \quad : \text{(Aromatics)} \tag{29}$$

Also the equilibrium constants for Eqs. (28) and (29) were determined by taking into account the overall stability constants, β, of cadmium chloride complex in the aqueous solution:

$K_{ex} = 3.60 \times 10^{-4}$ (*n*-Heptane) and 2.21×10^{-4} $(m^3/mol)^{0.5}$ (Kerosene);

$K_{ex} = 9.53 \times 10^{-7}$ (Toluene) and 9.32×10^{-7} (m^3/mol) (*m*-Xylene).

The total concentration of Cd(II) in aqueous chloride solution, $[Cd]^T$, is given by $[Cd]^T=[Cd^{2+}](1+\beta[Cl^-])$, where $\beta=3.2\times10^{-2}+1.46\times10^{-4}[Cl^-]$. Thus the distribution ratio, m_{Cd}, for the solution of *n*-heptane as the diluent is represented as

$$m_{Cd} = [\overline{Cd}]/[Cd]^T = K_{ex}[(\overline{HR})_2]^{2.5}/(1 + \beta[Cl^-])[H^+]^2 \tag{30}$$

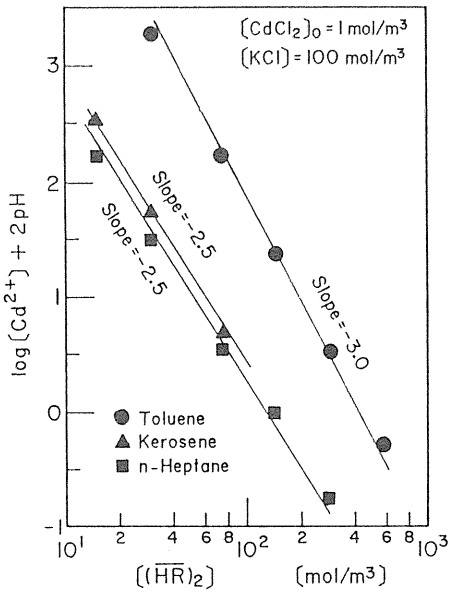

Fig. 2. 23. Plots of (log $[Cd^{2+}] + 2pH$) *versus* D2EHPA concentration $[(\overline{HR})_2]$ · ($[\overline{Cd}] = 0.1M$).

The extraction rates of Cd(II) by D2EHPA in *n*-heptane were obtained using a stirred vessel with a plane interface. The initial rate is proportional to the total concentration of Cd in aqueous phase and of D2EHPA in the organic phase, and inversely proportional to $[H^+]$, as shown in Fig. 2. 24. Assuming a rate-controlling step at the interface, we can interpret the respective concentration dependecies of the initial rate from the equation:

$$R_f = \frac{k_f[Cd]^T[(\overline{HR})_2]}{(1 + \beta[Cl^-])[H^+]} \tag{31}$$

where k_f was found to be 7.64×10^{-7} m/s.

The stripping rates, N_b, of cadmium from *n*-heptane solution containing Cd-D2EHPA complex by hydrochloric acid were obtained in the same stirred vessel as used for the extraction. As Fig. 2. 25 shows, the rate data were represented by

$$R_b = \frac{k_b[H^+][\overline{Cd}]}{[(\overline{HR})_2]^{1.5}} \tag{32}$$

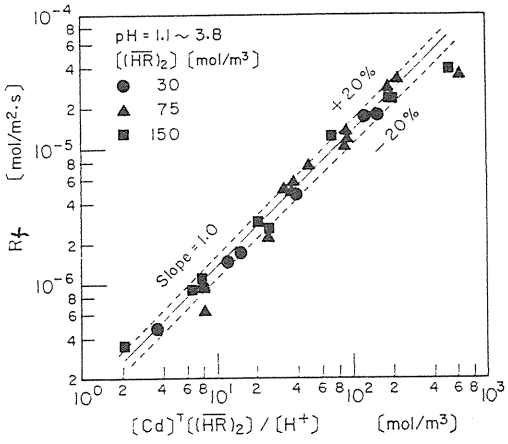

Fig. 2. 24. Correlation of the rates of Cd(II) extraction by D2EHPA.

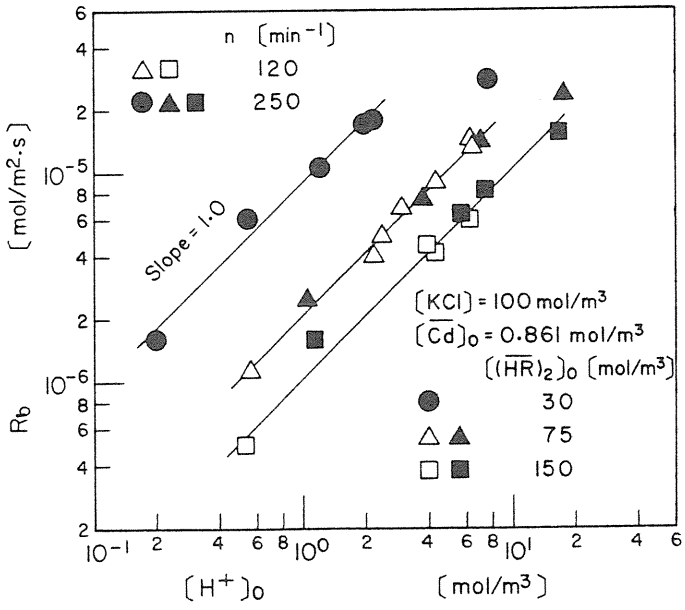

Fig. 2. 25. Effect of $[H^+]$ on the backward reaction rate for Cd(II).

Eq. (32) can also be derived from the reaction mechanism mentioned above; then, $k_b = 2.00 \times 10^{-3}\ (mol/m^3)^{0.5} \cdot (m/s)$. When Eq. (32) was coupled with Eqs. (30) and (31), the mass-action constant, K, for Eq. (28), defined by k_f/k_b, was found to be identical with the equilibrium constant, K_{ex}.

2. 3. 5. *Extraction of Gallium* (III) *by PC-88A*[35]

The equilibrium and kinetics for the extraction of Ga(III) from aqueous hydrochloric acid solutions by *PC-88A* in *n*-heptane were studied in the same ways as used in **2. 3. 4.** The extraction equilibrium was expressed by

$$Ga^{3+} + 2.5(\overline{HR})_2 \leftrightarrows \overline{GaR_3 \cdot 2HR} + 3H^+ \tag{33}$$

the equilibrium constant K_{ex} being found to be 2.0 $(mol/m^3)^{0.5}$.

The initial rates of the extraction and stripping are shown in Figs. 2. 26a and b as plots of $R_f[H^+]$ against $[(\overline{HR})_2]$ and [Ga] and of $R_b/[H^+]^2$ against $[(\overline{HR})_2]$ and $[\overline{Ga}]$, respectively.

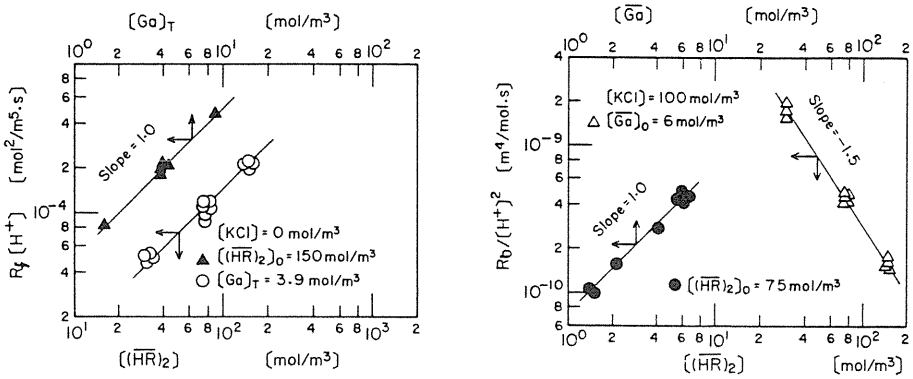

Fig. 2. 26. Correlation of the extraction rates for gallium by *PC-88A*.
a) forward extraction, b) backward extraction.

The concentration dependencies of both initial rates satisfy the assumption that a reaction between Ga^{3+} and ionic extractant species adsorbed at the liquid-liquid interface is likely to be the rate-controlling step. From Fig. 2. 26, we obtained both rate expressions for the forward- and backward-extraction reaction as follows:

$$R_f = k_f[Ga^{3+}][(\overline{HR})_2]/[H^+] \tag{34}$$

$$R_b = k_b[H^+]^2[\overline{Ga}]/[(\overline{HR})_2]^{1.5} \tag{35}$$

where k_f=3.80×10^{-7} m/s and k_b=5.0×10^{-8} $(m^3/mol)^{0.5}$(m/s).

2. 3. 6. *Extraction of Ti* (IV) *from Acidic Media by D2EHPA*[36]

The extraction equilibrium of Ti(IV) was studied between aqueous nitric acid solutions (0.1 ~ 6*M*) and *n*-heptane solution of D2EHPA at 25° and 50°C. The distribution ratio, $m(=[\overline{Ti}]/[Ti])$, is plotted in Fig. 2. 27 against $[HNO_3]$ at various initial concentrations of D2EHPA, $[(\overline{HR})_2]_0$. With increasing acid concentration, the *m* value decreases and goes through a minimum at the concentration of 2 ~ 3*M*. Such a behavior was also found in other acidic media; however, the extraction decreases in the order: $HNO_3 > HCl > H_2SO_4$.

Thus the extraction mechanism changed from a cation exchange reaction into a solvation reaction with increasing acid concentration. At low acidities it was found that the extraction reaction is expressed by

$$Ti(OH)_2^{2+} + (3/2)(\overline{HR})_2 \leftrightarrows \overline{Ti(OH)_2 \cdot HR_3} + 2H^+ \quad (36)$$

where the extraction constants were evaluated as $K_{ex}=2.63\times10^5$ $(mol/m^3)^{0.5}$ at 25°C and 4.79×10^4 (mol/m^3) at 50°C.

The kinetics of the extraction and stripping reaction was also examined in a dispersion system using a stirred vessel. Fig. 2. 28a shows the results of $R_f/[Ti][(\overline{HR})_2]$ obtained for the extraction as a function of the proton concentration, where $[(\overline{HR})_2]$ is the free D2EHPA concentration given by $[(\overline{HR})_2]_0-(3/2)[Ti]$; then, the line with slope -1.0 gives the rate equation for the forward reaction at 25°C as follows:

$$R_f = 3.5 \times 10^{-6}[Ti][(\overline{HR})_2]/[H^+] \quad (37)$$

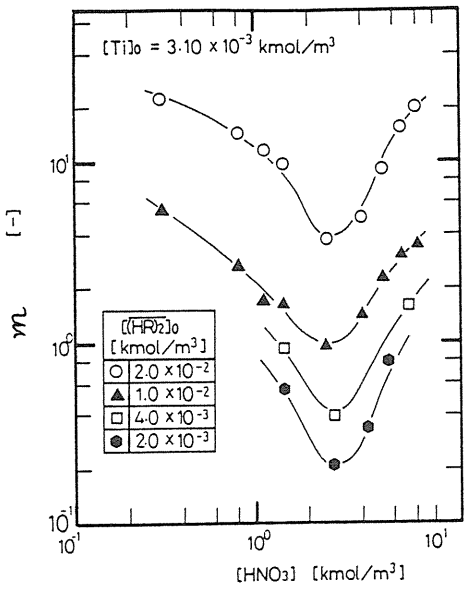

Fig. 2. 27. Distribution ratio of titanium(IV) as a function of HNO_3 concentration.

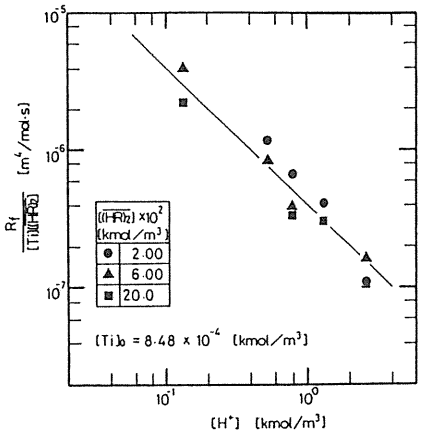

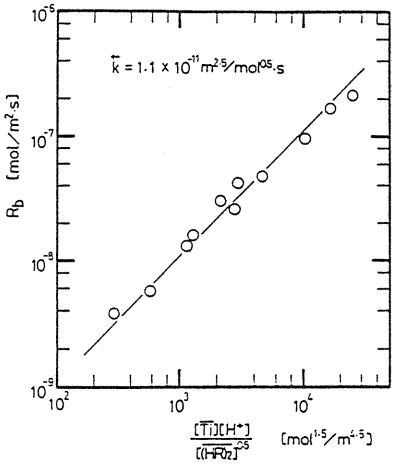

Fig. 2. 28. Correlation of the extraction rates for Ti(IV) by D2EHPA.
a) forward extraction (R_f), b) backward extraction (R_b).

On the other hand, typical results for the stripping are represented in Fig. 2. 28b as a plot of R_b versus $[\overline{Ti}][H^+]/[(\overline{HR})_2]^2$, whereby the effect of the forward reaction rate on the stripping rate is negligible. Thus the backward reaction rate can be expressed by

$$R_b = 1.1 \times 10^{-11} [\overline{Ti}][HNO_3]/[(\overline{HR})_2]^{0.5} \tag{38}$$

Both reaction kinetics of Eqs. (37) and (38) can be explained reasonably by assuming the rate-controlling step of a reaction between $Ti(OH)_2R^+$ and HR adsorbed on the interface. Furthermore assuming that the forward reaction rate is equal to the backward one at the equilibrium, we obtain the extraction constant as

$$K_{ex} = \frac{[\overline{Ti(OH)_2 \cdot HR_3}][H^+]}{[Ti(OH)_2^{2+}][(\overline{HR})_2]^{1.5}} = 3.2 \times 10^5 \tag{39}$$

This value is in good agreement with that from equilibrium data mentioned above.

2. 4. *Permeation Rate of Cadmium Through an SLM Containing D2EHPA*[37]

An illustrative example of coupled transport through an SLM is presented for the permeation of Cd(II) through a flat type SLM containing *n*-heptane solution of D2EHPA. The SLM module is identical with that used in **2. 1. 1**, composing from a *Millipore* filter (δ=125 μm, d_p=10 μm and ε=0.68). Cadmium was extracted from aqueous feed (I-side) by the SLM, and being back-extracted into the strip liquor (II-side) of hydrochloric acid (See Fig. 2. 1). The two aqueous solutions flowed concurrently on both sides of the SLM. We considered the following five consecutive steps.

Mass-transport rates of Cd^{2+} and H^+ through the aqueous boundary film on the feed side are given by

$$N_{AI} = k_{AI}([Cd]_I^T - [Cd]_{Ii}^T) \tag{40}$$

$$N_{AH} = -k_{HI}([H^+]_{Ii} - [H^+]_I) \tag{41}$$

where k_{AI} and k_{HI} are the mass-transfer coefficients for Cd^{2+} and H^+, respectively. At the surface on the feed side, if the extraction of Cd(II) proceeds at a rate given by Eqs. (31) and (32), we can then obtain the extraction rate, N_f, as

$$N_f = k_f\{\frac{[Cd]_{Ii}^T[(\overline{HR})_2]_{Ii}}{(1+\beta[Cl^-]_I)[H^+]_{Ii}} - \frac{[\overline{Cd}]_{Ii}[H^+]_{Ii}}{K_{ex}[(\overline{HR})_2]_{Ii}^{1.5}}\} \tag{42}$$

For the diffusion of the Cd-complex through the SLM, the membrane-transport rate can be expressed by

$$N_m = k_m([\overline{Cd}]_{Ii} - [\overline{Cd}]_{IIi}) \tag{43}$$

On the other side of the SLM, the cadmium is back-extracted by the strip liquor at a rate given from Eqs. (31) and (32); the stripping rate, N_b, is then obtained as

$$N_b = k_b \{ \frac{[\overline{Cd}]_{IIi}\,[H^+]_{IIi}}{[(HR)_2]_{IIi}^{1.5}} - \frac{K_{ex}[Cd]_{IIi}^{T}\,[(\overline{HR})_2]_{IIi}}{(1+\beta[Cl^-]_{II})\,[H^+]_{IIi}} \} \tag{44}$$

The transfer rates of both ions of Cd^{2+} and H^+ through the boundary film on the strip side are also expressed as

$$N_{AII} = k_{AII}\,([Cd]_{IIi}^{T} - [Cd]_{II}^{T}) \tag{45}$$

$$N_{HII} = -k_{HII}\,([H^+]_{II} - [H^+]_{IIi}) \tag{46}$$

Assuming an identical diffusivity for $(\overline{HR})_2$ and $(\overline{CdR_2 \cdot 3HR})$ as well as the negligible loss of the extractant into aqueous flows, we can obtain the concentration of the free extractant from a mass balance of D2EHPA in the membrane phase as

$$[(\overline{HR})_2]^T = [(\overline{HR})_2]_{Ii} + 2.5[\overline{Cd}]_{Ii} \tag{47-a}$$

$$= [(\overline{HR})_2]_{IIi} + 2.5[\overline{Cd}]_{IIi} \tag{47-b}$$

At a steady state, each rate for these five steps should be satisfied the following relation:

$$J_A = N_{AI} = N_{HI}/2 = N_f = N_m = N_b = N_{AII} = N_{HII}/2 \tag{48}$$

Thus the permeation flux of Cd(II), J_A, across the SLM can be obtained numerically from Eqs. (40) ~ (48). Fig. 2. 29 shows a plot of J_A vs. $[H^+]_I$ together with the calculated value (solid line). A good agreement in J_A is found between the observed and

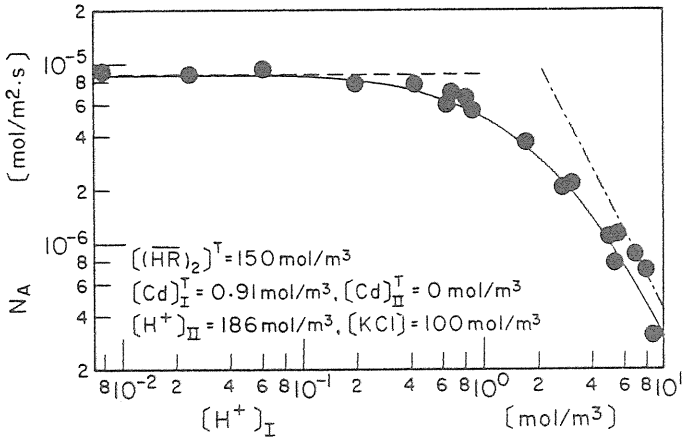

Fig. 2. 29. Effect of H^+ concentration in aqueous feed on the permeation flux of Cd(II). Solid line represents the calculated value from Eqs. (40)–(48); dashed line for aqueous boundary film-controlling on the feed side; dash-dotted line for the membrane diffusion-controlling.

calculated values. For $[H^+] < 0.1\,mol/m^3$, the value of J_A is independent of $[H^+]_I$. This suggests that the permeation is controlled by the diffusion through the aqueous boundary film on the feed side(I). With increasing $[H^+]_I$, J_A tends to approach the dash-dotted line.

Fig. 2. 30 shows the effects of both total concentration of Cd(II) in the aqueous feed and $(HR)_2$ in the membrane phase on J_A together with the calculated value (solid line), wherein the dashed line represents the diffusion-controlling through the aqueous boundary. The good agreement between the calculated and observed value of J_A implies that the permeation behavior across the SLM can be interpreted reasonably with the above-mentioned mechanism.

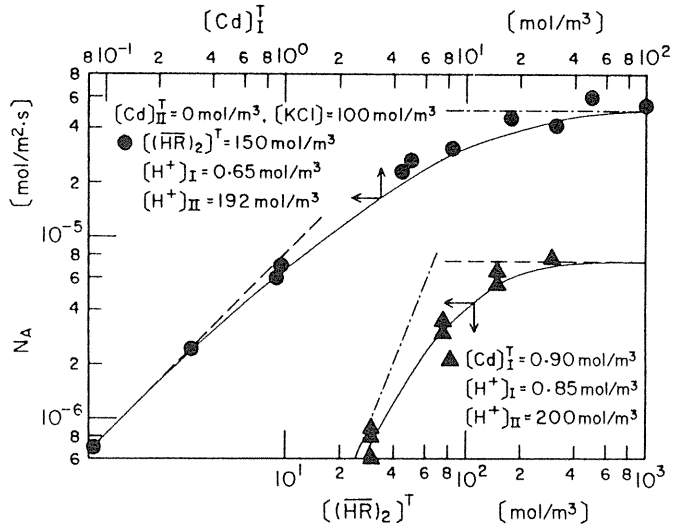

Fig. 2. 30. Plots of permeation flux of Cd(II) versus $[Cd]_i^T$ and $[(\overline{HR})_2]^T$. Solid, dashed and dash-dotted lines are the same as in Fig. 2. 29.

3. Stabilities of Liquid Membranes

3. 1. Supported Liquid Menbrane (SLM)

In SLM operations their lifetime, *viz.*, the membrane stability is a matter of great importance; however, there is very little information available. Although SLMs should be as thin as possible to minimize diffusion resistance, the membrane must be strong enough to withstand an appreciable pressure difference between feed and recovery sides, and it must hold sufficient solvent with an appreciable area for solute diffusion. Since the membrane solvent is held in the pore structure solely by capillary forces, it is inevitable that during the separation process the solvent and/or carrier is to some extent washed or forced out of SLM; in addition, dissolution may result in losses to the process stream. This will give rise to the imbibition of the solvent-water interface into the pores, and to a pinhole leak in the membrane, which will cause decrease in the separation performance of the SLM.

3. 1. 1. Breakdown Time of SLMs[38]

Some of the factors that influence the lifetime of SLMs were examined in terms of the leakage of water across the membrane. A schematic diagram of the experimental apparatus for studying a single hollow-fiber SLM is shown in Fig. 3. 1. Four commercially available HFs in Table 3. 1 were selected; the length of the fibers was in the range of 23 ~ 38 cm. As membrane solvents, four *C*-7 hydrocarbons were used in the experiments: *n*-heptane (aliphatics) and iso-heptane (its isomer); methylcyclohexane (naphtenes); toluene (aromatics); in addition, kerosene as a typical industrial solvent (mixture).

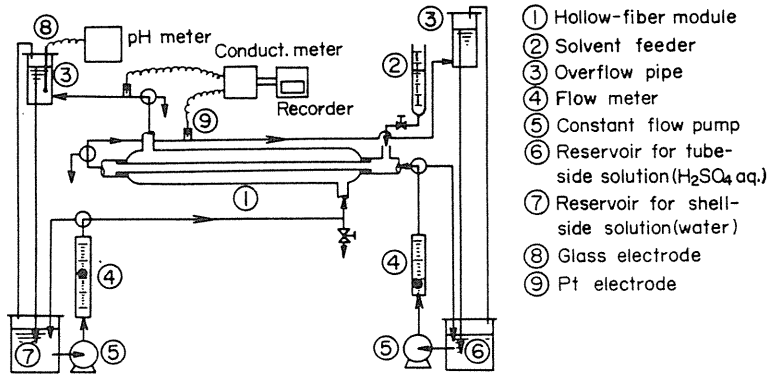

Fig. 3. 1. Schematic diagram of the experimental apparatus for study of hollow-fiber SLMs.

Table 3. 1. Hollow-fiber membranes used as solid supports.

Hollow fiber	Material	$\sigma_c^a \times 10^3$ (N/m)	Abbr.	I.D. (mm)	δ^b (μm)	Pore size (μm)	ϵ^c (%)
Gore-Tex TA001 (Gore-Tex)	teflon	18	PTFE	1.00	400	2[d]	50
Trial manufacture (Asahi Kasei)	polyethylene	31	PE(A)	280	0.05	—	
KPF-190M (Mitzubishi Rayon)	polypropylene	29	PP	0.20	22	(0.16)	45
EHF-207T (Mitzubishi Rayon)	polyethylene	31	PE(B)	0.27	55	(0.27)	70

[a]Critical surface tension. [b]Wall thickness. [c]Porosity.
[d]Max. size; ( ) estimated from bubble point.

In the experimental runs, a hollow fiber in the module was impregnated with an organic solvent, and diluted sulfuric acid (0.1*M*) was circulated through the inside of the HF at a linear velocity U_t; the outside stream consisted of deionized water at a constant velocity U_s, whereby a hydraulic pressure difference (Δh) was setup between the two channel streams.

From the time course of $[H^+]$, a curve of water leakage, R_L, as a function of time was determined, which will be termed the "*rate-of-leakage curve*" in the present study.

Fig. 3. 2. shows typical rate-of-leakage curves for the two *PTFE* and *PP* fiber SLMs. The lifetime of the *PTFE* membrane is longer than that of the *PP* membrane; however, toluene is liable to be forced out of the SLM, while either *n*-heptane or kerosene sorbed into the *PTFE* fiber allows a lifetime of more than few days even under conditions of Δh=20 cm-H_2O. The breakdown times, t_B, were given in Table 3. 2, which were determined as the point at which the curve rises up from the line R_L=0. The value of t_B may be taken as a relative measure of SLM stability; if this is true, the following sequence was observed for *C-7* hydrocarbons:

Aliphatics > aliphatic isomers, naphtenes >> aromatics.

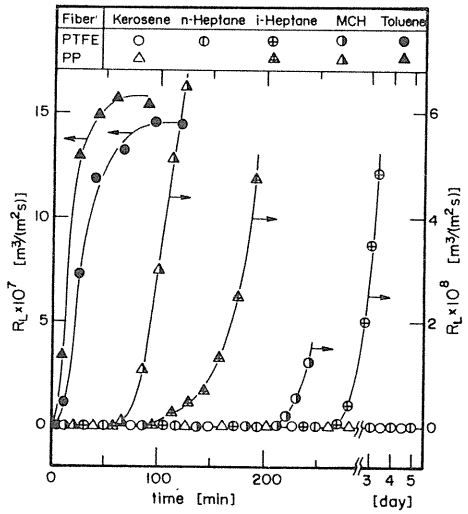

Fig. 3. 2. Plots of the apparent leakage rate of water across hollow-fiber SLMs as a function of time (Δh = 20 cmH_2O, U_t = 10 − 13 cm/s, U_s = 20 cm/s).

Further experiments were conducted using flat-sheet SLMs, in order to elucidate the effects of pressure difference, pore structure and solvent properties on the stability of the SLMs. The same device as in ***2. 1.1*** was employed together with microporous membranes shown in Table 2. 2. The typical results for the lifetimes of three SLMs are shown in Fig. 3. 3 as a plot of R_L *vs. t.* Although the pores of *Nuclepore* are essentially straight-through holes, in evident contrast to the matrix pore structures of *Duragard* and *Fluoropore*, its SLM has a comparatively long lifetime at low ΔP. These SLM characteristics show the influence of pore morphology and solid support material on the stability, even though the three sheets are of different thickness.

Table 3. 2. Breakdown times of HF-SLMs impregnated with organic solvents. (Δh = 20 cmH_2O, U_t = 10—13 cm/s, U_S = 20 cm/s).

Hollow fiber	Breakdown time[a], t_B (hr)				
	n-Hep.	Ker.	i-Hep.	MCH	Tol.
Teflon	> 120[b]	> 120[b]	4.1	3.5	0.05
PP	-	48	1.7	1.4	0.2
PE(A)	82	> 100[b]	16	10	0.7
PE(B)	-	75	3.5	2	0.1

[a]n-Hep., n-heptane; Ker., kerosene; i-Hep., iso-heptane; MCH, methylcyclohexane; Tol., toluene.
[b]Stability test was discontinued after 100 or 120 hr.

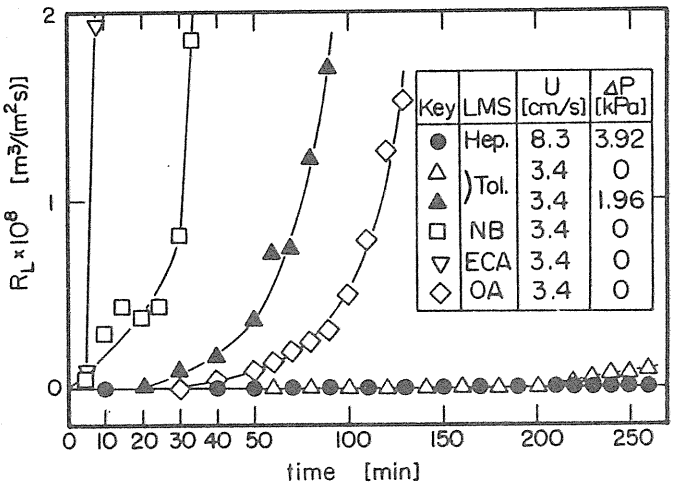

Fig. 3. 3. Plots of the apparent leakage rate of water across *PTFE* flat sheets (*FP*-200) with five different solvents as a function of time. Membrane solvent: *Hep.*, *n*-heptane; *Tol.*, toluene; *NB*, nitrobenzene; *ECA*, ethyl chloroacetate; *OA*, *1*-octanol.

3. 1. 2. Mechanism of Breakdown of SLMs[38,41]

Membrane liquid is held within the pores of polymeric solids by a capillary force, $P_c=(2\gamma/a)\cos\theta$, according to Young-Dupre' equation. However, when the contact angle, θ, of organic liquid to water phase is less than 90°, the organic-water boundary (the surface of SLM) imbibes into the SLM and then the membrane phase is displaced with the aqueous phase. Rate of the imbibition, q, of such a three phase boundary into a pore filled with membrane liquid can be expressed by the Rideal-Washburn equation;

$$q = a\gamma\cos\theta/4\delta\mu \tag{49}$$

where a is the pore radius, μ the viscosity of the imbibing liquid (aqueous solution), and γ the interfacial tension. From viewpoints of P_c and q, the pore size has the most significant effect on the stability of SLMs.

We here considered metal separation using an SLM with an extractant as the carrier. The three-phase boundary tends to penetrate into the SLM from the feed side (upstream) to the strip liquor side (downstream), provided that the metal-extractant complex formed at the interface on the upstream side lowers the interfacial tension. Measurements were made on the interfacial tension between aqueous and *n*-heptane solutions under conditions of Ni(II)- and Co(II)-extraction by D2EHPA(HDEHP) and *PC-88A*(EHPNA). Fig. 3. 4 shows the effect of metal-loading ratio in the organic phase on the γ-value during the extraction at *pH*4, wherein the dashed and dotted lines represent those in equilibrium for the systems of Co-EHPNA(1), Ni-EHPNA(2) and Ni-HDEHP(3).[41] For the Ni-extraction, the value of γ lowered with increasing metal loading in the organic phase, unlike the Co-EHPNA system. In addition, these values are smaller than those obtained under no-reaction conditions. On the other hand, no significant change in γ during the back-extraction was observed for any of the systems. Thus, to ensure the stable operation in the SLM separation, it is desirable to adopt

the downstream on the skin-layer side under pressure conditions, provided that the solid support is asymmetrical.

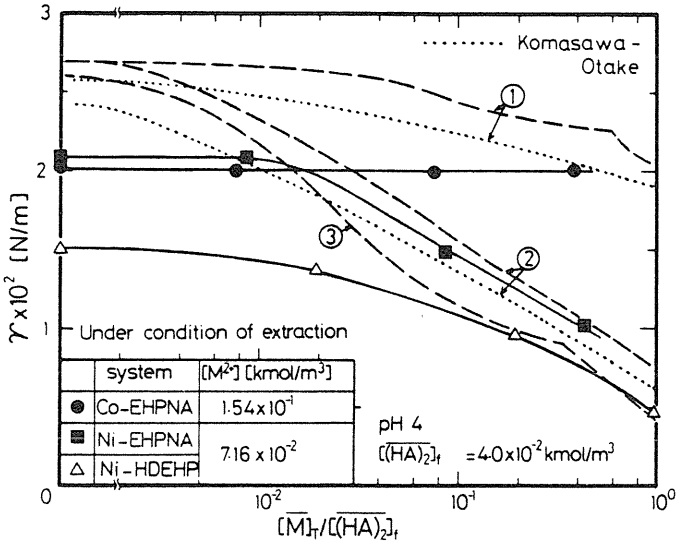

Fig. 3. 4. Effect of metal loading ratio in the organic phase on the interfacial tensions under conditions of metal extraction by HDEHP and EHPNA in *n*-heptane. Dashed and dotted lines represent the interfacial tensions in equilibrium: ① Co-EHPNA, ② Ni-EHPNA and ③ Ni-HDEHP systems.

3. 1. 3. Progressive Wetting of SLMs by Aqueous Solution[39]

Kim and Harriott[42] discussed the minimum entry pressure for water into a *PTFE* membrane with and without impregnation by an organic in terms of an effective contact angle, θ_{eff}, giving anomalously low entry pressure. In other words, an SLM allows water to be imbibed below a critical pressure difference by the Young-Dupre's eq. The progressive wetting by an aqueous solution of an SLM thus presents an important problem in SLM operations. Here, consideration was given to a submerged aqueous drop on a horizontal porous sheet in an organic solution, as shown in Fig. 3. 5. The work of immersional wetting may be defined in a way similar to that for drops on a non-porous plate,

$$W_i = \gamma_{so} - \gamma_{sw} = \gamma_{ow} \cos\theta \tag{50}$$

With a contact angle $\theta \geq 90°$ and $W_i \geq 0$, the wetting becomes immersion; therefore, the liquid-liquid interfacial tension γ_{ow} has an influence on the wettability due to the difference between $\gamma_{(s/o)\text{-}o}$ and $\gamma_{(s/o)\text{-}w}$, which can only be expressed by $\gamma_{ow} \cos\theta$.

Contact angle was determined by measuring the height of small aqueous drop (2 or 8 μl) on a polymeric sheet in contact with a sintered glass plate placed horizontally within a spectrophotometric cell filled with an organic solution. Three microporous sheets were used: *FP*-100, *Duragard* 2500 and *Nuclepore* membranes. As the organic liquid, *n*-heptane, toluene,

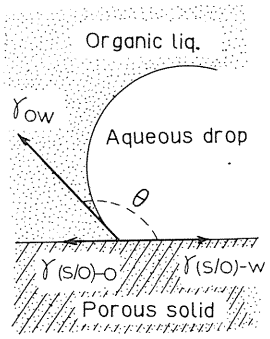

Fig. 3. 5. Schematic representation of aqueous drop on a horizontal porous sheet, submerged in an organic solution.

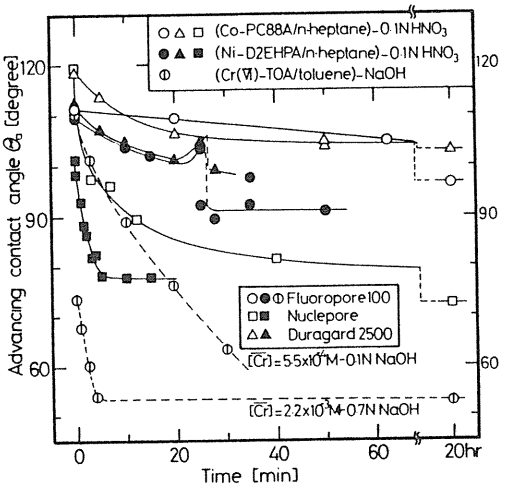

Fig. 3. 6. Variation of contact angle as function of elapsed time.

and kerosene were used as well as their solutions of three extractants of D2EHPA, *PC-88A* and TOA.

Values of θ for both toluene and kerosene showed a slight decrease with elapsed time; similar behavior was also observed during the extraction of metal ions, with no significant difference. However, in actual SLM for the Ni-(D2EHPA/*n*-heptane) and Cr-(TOA/toluene) systems, the lifetime were comparatively short, as discussed in ***3. 2. 2.*** Thus, further measurements of θ were conducted under conditions of back-extraction:

(A) (D2EHPA/n-heptane) loaded with $Ni(NO_3)_2$-0.1N HNO_3; concentrations of D2EHPA and of Ni in the organic phase, $[\overline{(RH)_2}]=0.04M$ and $[Ni]=0.04M$, respectively.

(B) (PC-88A/n-heptane) loaded with $Co(NO_3)_2$-0.1$N$$HNO_3$;$[\overline{(RH)_2}]=0.04M$ and $[\overline{Co}]=7.3mM$.

(C) (TOA/toluene) loaded with $K_2Cr_2O_7$-0.1NNaOH; $[\overline{TOA}]=0.027M$ and $[\overline{Cr(VI)}]=0.55mM$.

Typical values of θ for the three different membranes are plotted in Fig. 3. 6 as a function of the elapsed time. It is to be noted that system A exhibited pronounced turbulence due to the Marangoni effect unlike system B, and system C gave the rapid change in θ. As a means of inferring the time required for complete wetting of SLMs by aqueous solution, the values of $\gamma\cos\theta$ for the three systems are plotted in Fig. 3. 7 against the elapsed time; the broken lines represent the respective values of γ corresponding to $\cos\theta=1$. The point of intersection of the extrapolated line (dashed-and-dotted line) through the data points with the broken line may thus be defined as a "*critical wetting time*", t_c, which can be used as an index of the progressive wettability and, therefere, of the effective lifetime of an SLM.

The value of t_c for system A decreases the following sequence: *Duragard 2500, FP-100, Nuclepore*; system B gives a large value even with *Nuclepore.* The result for system C suggests that, even with *FP-100,* the SLM is so unstable that it is replaced by the aqueous solution within 120 to 200 *minutes.* However, in practical SLM separation, membrane breakdown may quite probably be caused in a shorter time by the pressure difference between the two

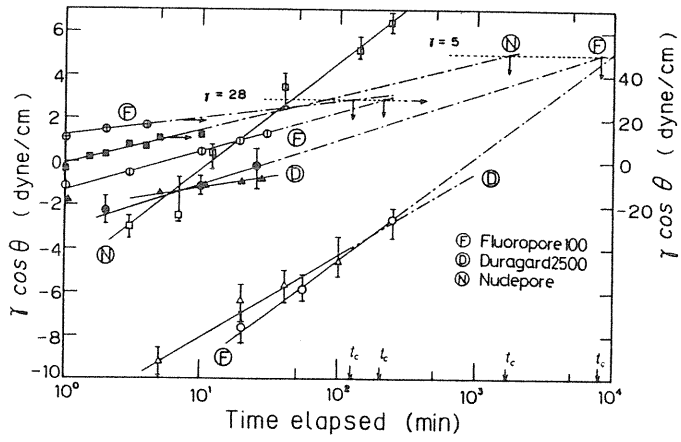

Fig. 3. 7. Results of wetting studies.

sides of SLM. It can be concluded that the relative lifetime based on the progressive wettability of an actual SLM can be evaluated in terms of critical wetting time from a plot of $\cos\theta$ versus t.

3. 2. *Methods for Continuous Regeneration of SLMs.*

In SLM operation, it is necessary to makeup the membrane liquid, because the solvent and/or carrier is to some extent washed or forced out of the SLM. Some methods for the continuous regeneration have been examined: (1) Mixed-flow mode of the membrane liquid together with the strip liquor, (2) forced feeding mode under a reduced pressure, (3) penetrating flow mode due to the capillary action, (4) creeping-flow mode due to both forces of the capillary action and buoyancy, (5) flowing liquid membrane and (6) contained liquid membrane mode. We have proposed two methods of (1) and (4); these views were demonstrated.

3. 2. 1. *Mixed-Flow Mode of Membrane Liquid*[43]

An SLM device shown in Fig. 3. 8 was used in which an organic membrane solution is forced to flow with aqueous strip liquor on one side of the SLM: a hybrid liquid membrane of bound and supported types. *Nuclepore* membrane was employed as the solid support. Copper was extracted with the refined LIX65N in kerosene ($[\overline{RH}]_0$=0.049M) from aqueous feed of $CuSO_4$ ($C_{w,in}$=1mM and pH_{in}=5.5), being then stripped by dilute H_2SO_4 (0.93M) at the surface on the other side of the SLM. The velocity of the aqueous feed, U_F, ranged from 0.007 to 0.15 m/s, whereas that of the strip liquor was 0.005 m/s. Pressure on the feed side was kept about 15 cm-H_2O higher than that on the strip side to avoid leakage of the membrane liquid into the aqueous feed flow. The superficial velocity of the membrane liquid was 0.005 m/s.

The value of pH in the feed decreases with proceeding of the Cu(II) permeation, owing to the ion-exchange reaction by Eq. (14). The pH change in the effluent on the feed side is shown in Fig. 3. 9. A somewhat different course in the pH change was observed when the injection of the membrane liquid on the strip side was stopped (t=0), whereby the pH value became constant after going through a minimum. The removal efficiency

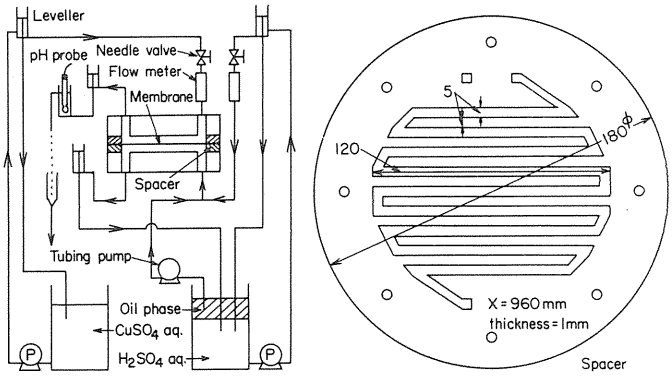

Fig. 3. 8. Schematic diagram of experimental apparatus and details of spacer for liquid flow channel.

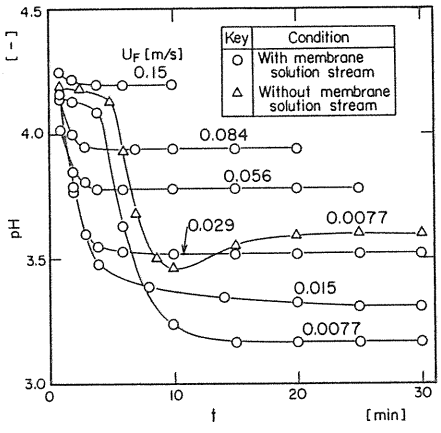

Fig. 3. 9. Time course of *pH* in effluent of feed solution.

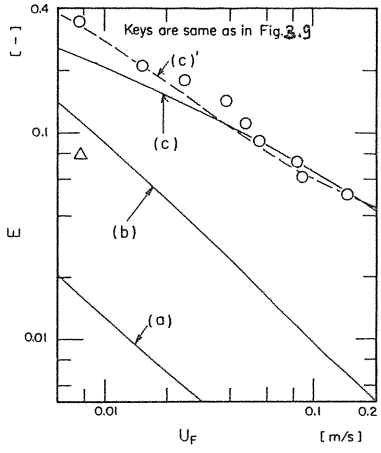

Fig. 3. 10. Comparison between experimental and calculated values of copper permeation fraction.

E (= $1-C_{W,out}/C_{W,in}$), of Cu(II) at a steady state is plotted in Fig. 3. 10 against U_F, wherein lines represent the calculated values mentioned below. To attain an efficient removal, a large SLM length, a small channel depth (i.e., large specific surface area) and a small U_F are required, as can be seen in Fig. 3. 10. Also, it is to be noted that there is a difference of about four fold in E between the runs with and without the forced flow of the membrane liquid. This mixed-flow mode with the strip liquor is useful for enhancing the permeation rate of Cu(II) as well as stabilizing the SLM.

Since the membrane liquid was added periodically to the strip liquor, it flowed as a lump filling up the strip channel. The oil lump is broken up into smaller ones as it flows through the channel; the surface on the strip side of the SLM can then be swept by the oil stream. By considering this situation, three calculations for the Cu(II) permeation through the SLM were

done as follows. *Case*(*a*): the membrane liquid exists only within the pores of the solid support; the shape of the interface reflects the pressure difference across the SLM. *Case*(*b*): the surface on the strip side is covered with the membrane liquid; thus, the stripping reaction occurs at the whole surface, and mass-transfer resistance through the oil layer was neglected in the present calculation. *Case*(*c*): the membrane liquid is interchangeable between the membrane phase and the stream on the stripping side.

The calculation results for the present experimental conditions are shown in Fig. 3. 10 with the lines(*a*), (*b*) and (*c*) for *cases*(*a*), (*b*) and (*c*), respectively. The dashed line(*c*)' represents a correction of *case*(*c*) by using $k_w=8.8\times10^{-5}$ $(0.1+U_w)$. The E value for *case*(*a*) is less than one-tenth that for *case*(*c*); the ratio of E for *case*(*b*) to (*a*) is nearly equal to that of the effective areas on the strip side. A good agreement in the E values was found between the observation and the calculation for *case*(*c*)', indicating that the Cu(II) concentration at the surface on the strip side is kept very low by sweeping its surface with the membrane liquid. In conclusion, the diffusion resistance through the aqueous boundary film on the feed side is appreciable for the Cu(II) transport across the SLM.

3. 2. 1. Creeping-Flow Mode due to Capillary Action and Buoyancy[17,44)]

A method of continuous regeneration (*CR*) for HF- SLMs was proposed, which utilizes the capillary action and buoyancy force of organic liquid within the continuum pores of the polymeric support, and the membrane stability was demonstrated in permeation tests through the SLM modules.

The structures of the two *CR*-SLM devices used in the present study are shown in Fig. 3. 11: single-HF and multi-HFs modules. Membrane liquid penetrates into the pores of HF from a liquid located at the bottom section, then moving up through the pores or creeping on the lumen side of the vertical fiber by buoyancy force and capillary action. Five commercial available HFs were selected; the composition and specification of each fiber are given in Table 3. 1. The multi-HFs module (Fig. 3. 11b) is composed of a tube bundle contained over 38-HFs (15 cm in length) and a transparent *PVC* pipe (8 cm *i.d.*) as a shell tube. All the HF tubes were passed through six ceramic cross-baffles (thickness: 0.8 mm) and sticked out both ends of them at the top and bottom plates. In all the experimental runs aqueous feed flowed

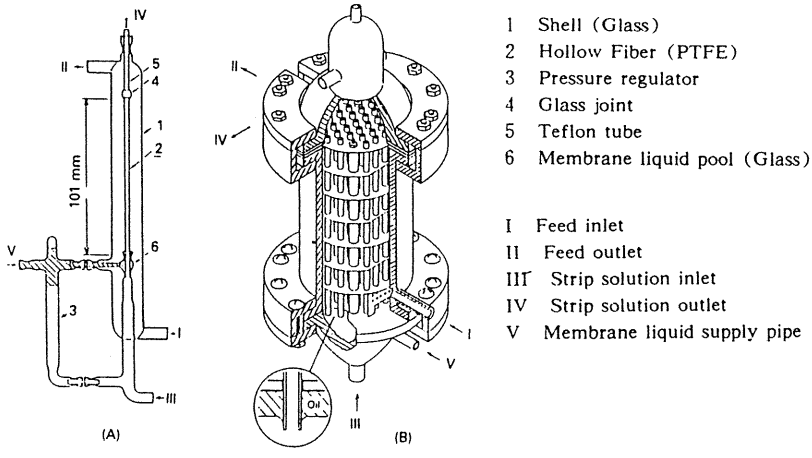

Fig. 3. 11. Two hollow-fiber SLM devices used in this work.

on the outside of the HFs (shell side), whereas the receiving phase (strip liquor) on the lumen side. Measurements were conducted on the permeation of Ni(II), Co(II) and Cr(VI) across the *CR*-SLM for the following three extraction systems: (1) Ni(II)-(HDEHP/*n*-heptane), (2) Co (II)-(EHPNA/*n*-heptane) and (3) Cr(VI)-(TOA/toluene or kerosene).

Fig. 3. 12 shows typical results obtained in the two SLMs for *system* (*1*), which forms a less stable SLM. In the nonregenerating mode, a decline in the permeation flux begins after a short period of time, in contrast to the breakdown time of *ca.*12 hrs for water. Such a behavior is probably because the Ni-complex contains water molecules as a ligand and the water is liberated from the complex in the membrane during the diffusion in accordance with equilibrium between the complexes. In the case of the *CR*-SLMs, on the other hand, the fluxes of Ni(II) were maintained at a constant value over the entire one-week duration of the experiment; further, the *CR*-SLM of the *type A* was found to be stable for both systems of (*1*) and (*2*) over a half month.

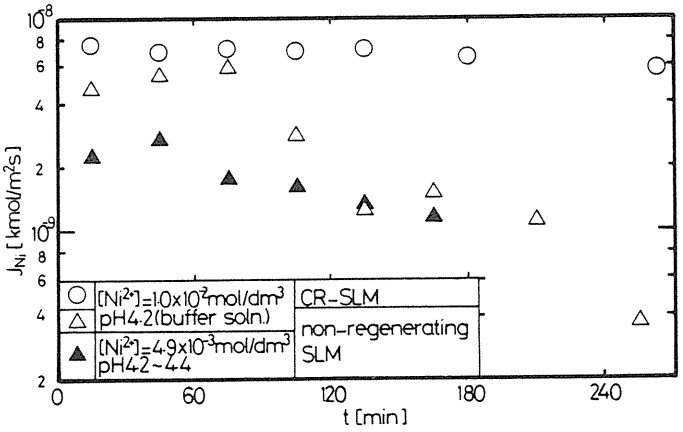

Fig. 3. 12. Plots of permeation flux of nickel against operation time for SLM with *n*-heptane solution of HDEHP (0.08*M*).
Feed solution, U_s = 5 cm/s; strip solution, HNO_3 $1.0\times10^{-2}M$, U_t = 3 cm/s.

Aromatics are likely to be washed or forced out of SLM, as described in ***3. 1.*** Thus, when considering the separation of Cr(VI) from an acidic medium by an SLM with TOA, as an illustrative example, the selection of its diluent becomes a serious problem, because Cr(VI)-TOA complexes have a tendency to form aggregates in aliphatic solvents.[45] Fig. 3. 13 shows that the aggregates formed in kerosene as the membrane liquid allow to lower the permeation flux of Cr through the SLM, while a significant improvement in the permeation is found by use of the *CR*-SLM with TOA in toluene. Also the addition of *1*-octanol to kerosene prevents the aggregation of Cr-TOA complexes; however, the non-regenerating SLM gives an upper limit in the flux at a "*critical concentration*" for the aggregation as well as that without *1*-octanol. With increasing concentration of Cr(VI) in the aqueous phase, the permeation flux across the *CR*-SLM with the toluene solution tends to converge to the line of the slope 0 in Fig. 3. 13. This suggests that the permeation behavior can be interpreted from mass transfer resistances through the external aqueous boundary film and the oil-containing

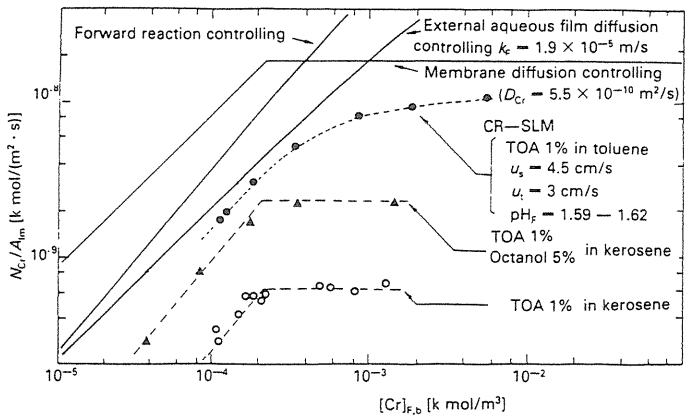

Fig. 3. 13. Effect of membrane solvent as a diluent of TOA on the Cr(VI)-permeation across the SLM with and without the regeneration.

membrane layer, represented by the solid lines.

3. 3. *Emulsified Liquid Membrane (ELM)*

In general, the (*W/O*)-drops in (*W/O*)/ *W*-double emulsions are of the size ranging from several μm to few hundred μm, whereas the inner water droplets less than several μm. In (*W/O*)/ *W* dispersion systems under a shear flow, the (*W/O*) emulsion drops are exerted to varying degrees of inertial and viscous forces; the drop deformation for the breakup is then brought about. In addition, double-emulsion breakup is caused by the swelling from water permeation in the presence of an osmotic pressure gradient. This phenomenon may be more significant with an increase in the enrichment ratio, where water permeates from the continuous phase (dilute feed) to the inner aqueous drop phase (concentrated receiving solution).

3. 3. 1. *Mean Drop Diameters of W/O- and (W/O)/W-Dispersion in an Agitated Vessel*[46]

Diameters of drops in an agitated vessel with one or two impellers were measured for water drops dispersed in kerosene, (*W/O*)-emulsion, and (*W/O*)-emulsion drops in water, (*W/O*)/ *W*-dispersion, in the presence of Span80 as an emulsifying agent. Fig. 3. 14 shows the typical results obtained for the drop size distributions with a parameter of the agitation speed, *N*, at a Span80 content, C_s, of 1 *wt*%, indicating that those can be expressed by a logarithmic normal distribution. The Sauter mean diameters, d_{32}, of the drops for the (*W/O*)- and (*W/O*)/ *W*-dispersion systems depend on *N*, impeller diameter and C_S. The dependence of d_{32} on C_s corresponds to the variation of the value of γ obtained under dynamic conditions, as shown in Fig. 3. 15. The d_{32} values obtained for the (*W/O*)/ *W* dispersion are plotted in Fig. 3. 16 against the Weber number, $We=D_i^3N^2\rho/\gamma$, wherein the solid line represents

$$d_{32} = 2.4 \times 10^4 \ We^{-0.95} \tag{51}$$

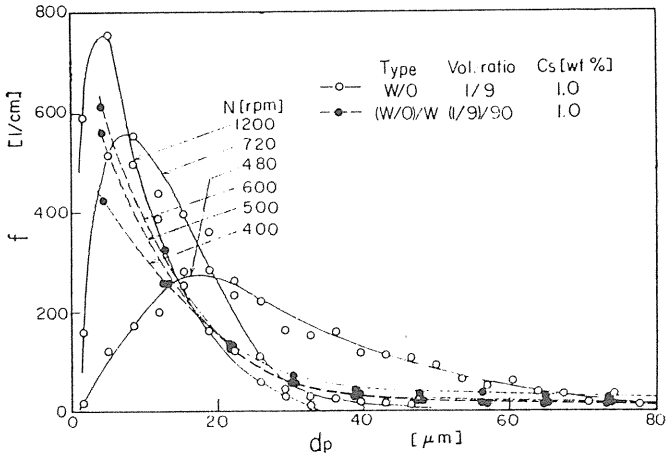

Fig. 3. 14. Drop size distributions of water drops in oil and of *W/O*-emulsion drops in water.

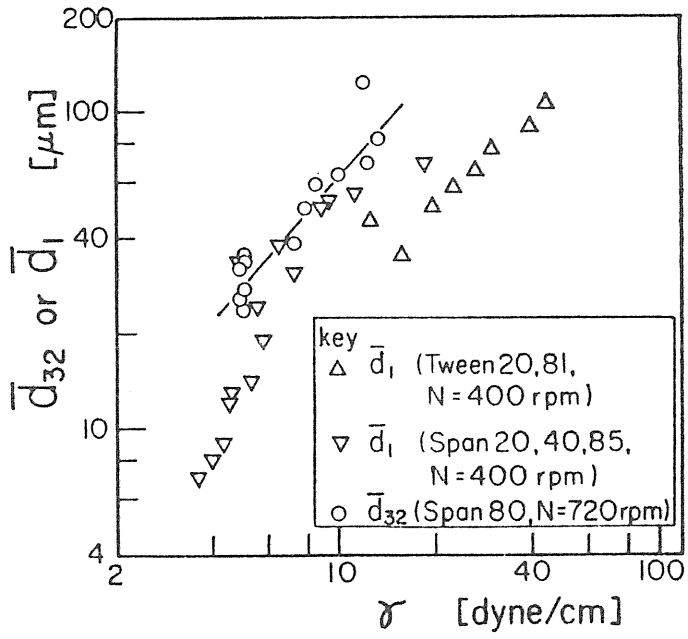

Fig. 3. 15. Effect of interfacial tension on mean drop diameter.

and the dashed line is from a previous correlation for (*W/O*)-dispersion system without emulsifying agent. This agreement implies that water droplets dispersed in kerosene scarcely coalesced in the presence of Span80; thus, the drop size distribution did not vary with the dispersed phase holdup fraction. For smaller C_S, however, the drop size decreased from lowering of the surfactant concentration per unit interfacial area.

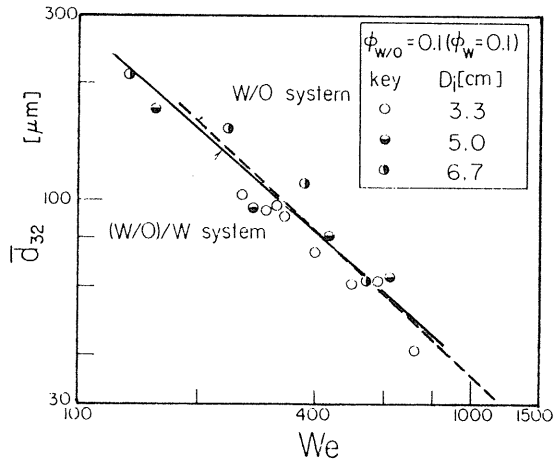

Fig. 3. 16. Correlation of Sauter mean diameter of *W/O*- emulsion drops in water.

3. 3. 2. Phase Inversion in Liquid-Liquid Dispersion[47)]

To attain an efficient contact between two liquid phases in dispersion, it is advisable to operate at high fractional volume of the dispersed phase, ϕ_d, as well as small size of dispersed drops. However, when making the dispersed holdup higher, phase inversion is liable to take place at a value of ϕ_d, and then there is an ambivalent range as a hysterisis depending on the original type of the dispersion (*W/O* or *O/W*). A study was made on the phase inversion caused by adding more dispersed phase into a liquid-liquid dispersion in a stirred tank with a six-bladed turbine.

Typical results for kerosene-water glass solution system are shown in Fig. 3. 17, whereby

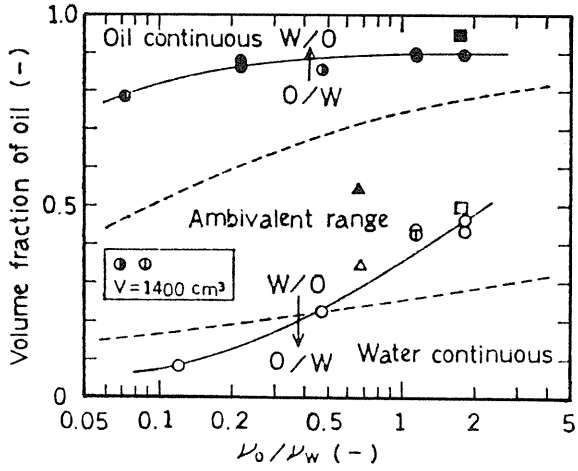

Fig. 3. 17. Phase inversion characteristics for kerosene-water glass solution system (Ranges of *P/V* are in 1.98–3.22 and 0.57–3.36 for top and bottom solid line respectively.) ○○●○ this work; ——— Selker et al. (various systems); △ ▲Clarke et al. (toluene-water); □■ Ali(kerosene-water).

the ambivalent range varied from 10% dispersed oil franction to 90% with an increase in the kinematic viscosity of water phase. Fig. 3. 18 shows the results for kerosen-water system in the presence of Tween20 as a surfactant, indicating that the behavior of inversion from the *W/O*- to *O/W*-dispersions gives a critical point at the *CMC* value of the surfactant, as well as the interfacial tension, γ, of the system.

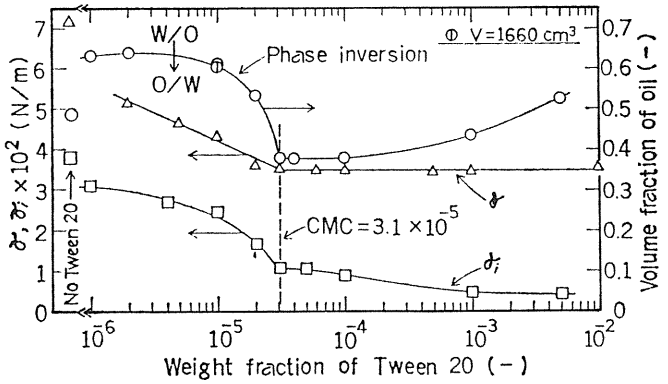

Fig. 3. 18. Phase inversion behavior as compared with surface and interfacial tensions for the system kerosene-Tween20 aq.solution ($N = 4.05$ rps).

3. 3. 3. *Breakage of ELMs*[48,49]

The breakdown of ELM comes from the deformation of (W/O) droplet under shearing conditions as well as the swelling due to water permeation through the thin oil-layer. The breakdown was determined by measuring the quantity of a trace-ion leaked out from the inner dispersed droplets into the continuous phase under fixed conditions. Then the breakdown ratio was defined by

$$\varepsilon = C_e V_e / C_{i,o} V_{i,o} = C_e(1-\Phi)/ C_{i,o}\Phi\phi \tag{52}$$

where C is the tracer concentration, V being the volume of aqueous solution; the subscripts e, o and i represent the outer and inner phases, and the initial state, respectively. Φ and ϕ are the volume fraction of inner water in (W/O) droplet and of the (W/O) emulsion in (W/O)/W dispersion, respectively.

From a viewpoint of the ELM separation, the breakdown of emulsion drops was measured for a Span80-kerosene system over a wide range of pH using $CuSO_4$ and NaSCN as the tracer in the presence of H_2SO_4 and NaOH. Fig. 3. 19 shows the effect of pH on ε, indicating that the solution

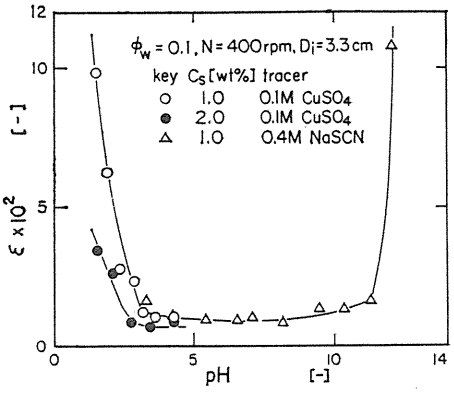

Fig. 3. 19. Variation of breakage fraction with pH in inner aqueous phase.

more alkaline than $pH11.5$ causes a drastic increase of the membrane breakdown, whereas for $pH<3$ there is also a significant increase in the ε-value. It was found that the stability of the $(W/O)/W$ emulsion depends on the ionic species and its concentration in the inner aqueous phase; in other words, the osmotic pressure gradient between the inner and outer aqueous phases is crucial for the membrane stability.

Furthermore, the breakdown ratio of an ELM during copper extraction is plotted in Fig. 3. 20 against the content of LIX65N in kerosene, whereby the value of ε_{60} at the contact time of 1 hr was evaluated by means of a trial and error with the values of $C_{w,o}$ and pH. The value of ε_{60} increases with the LIX65N content, and then became higher than that in the case without extraction by a factor of 2. Such a behavior may also be caused by a change in the interfacial tension as illustrated in Fig. 3. 21. The interfacial behavior between the Span80

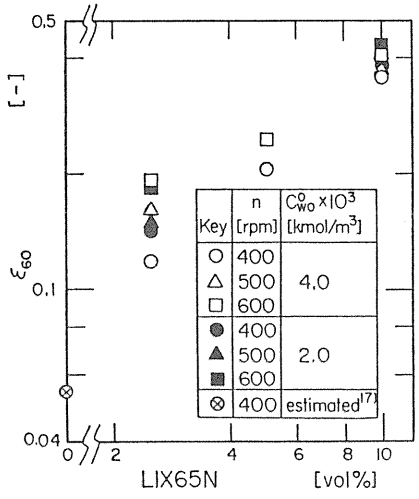

Fig. 3. 20. Plots of breakeage fraction of liquid membrane vs. LIX65N concentration.

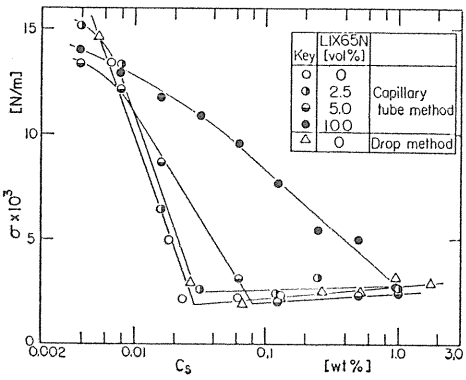

Fig. 3. 21. Effect of Span80 content on interfacial tension for LIX65N-kerosene water system.

solution and water phase varied greatly with the LIX65N content, especially the raise in the critical micellaneous concentration of Span80 is remarkable. Thus, simultaneous measurement was made on the membrane breakdown and water uptake in the (W/O) drops for various $(W/O)/W$-dispersion systems.

3. 3. 4. Effect of Organic Solvents on the Stability of ELMs[50–52]

A stirred cell consisting of a glass vessel of 6 cm ID and 13 cm height, fitted with four baffles, was used for dispersing (W/O) emulsion in an aqueous phase. Agitation was performed by a magnetic stirrer, in which a stirring bar made of Teflon was employed, with expectation that mechanical breakdown of (W/O)-droplets may be suppressed. (W/O) emulsion was prepared by mixing an organic solvent contained Span80 of 3 wt% and an aqueous solution of $Ni(NO_3)_2$(1000 ppm Ni^{2+}). To set an osmotic pressure gradient, an appropriate amount of H_2SO_4 was added to the aqueous solution.

Fig. 3. 22 represents the change in $V_i/V_{i,o}$ for the (W/O)-emulsions consisting of kerosene and toluene. In all cases under isotonic conditions, the $V_i/V_{i,o}$ value becomes constant

after an elapsed time of 5 *min*; thus, no water permeation through the membrane is observed. This suggests that the entrainment of external water into the (W/O)-drops is likely to occur only during the initial period of the contacting, especially in the absence of electrolyte. Such a secondary emulsification may be due to the excess of surfactant in the primary emulsification. However, the existence of electrolyte in the external aqueous phase has a tendency to suppress the secondary emulsification, as shown in Fig. 3. 23.

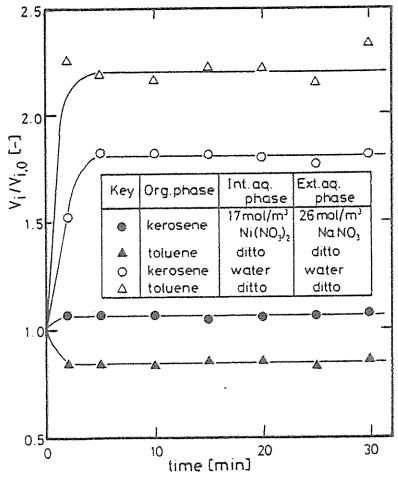

Fig. 3. 22. Changes in volume of (W/O) droplets with time elapsed under isotonic conditions, using kerosene and toluene as membrane solvent.

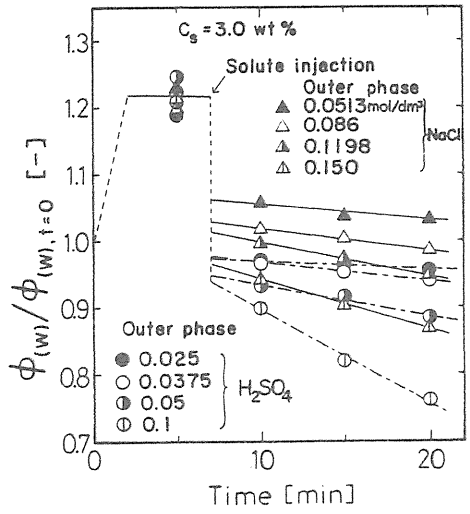

Fig. 3. 23. Time course of ϕ_W for water permeation from inner to outer W-phase. ($\phi_{W,t=0} = 0.55$).

Typical results of ε for various solvents is shown in Fig. 3. 24 against the contact time. Values of the time-dependent ε decrease with an increase in the number of carbon atoms among the aliphatics; however, the ε-value for toluene is about twenty times that for kerosene. Thus we conclude that more stable SLMs can be attained by use of a higher aliphatic hydrocarbon as the membrane solvent, and that aromatics tend to be easily broken down under shearing conditions.

Here, the breakdown of (W/O)-emulsion drops was disussed in terms of the surfactant concentration per unit interfacial area, q_s, evaluated from

$$q_s = (C_s/100)(\rho_o/M_s)(1-\phi)\Phi\, V_T/A_T \tag{53}$$

where M_s is the molecular weight of Span80 (=604), ρ_o the density of the organic solution, V_T the total volume of (W/O)/W dispersion. Fig. 3. 25 shows the effect of q_s on the breakdown ratio, where the decrease in q_s is attributed to an increase in the interfacial area from water permeation through the membrane, and hence the breakdown increased with time. In the region of small q_s value, these plots give a linear relation; the line can then be extrapolated to a point which allows ε=1 when q_s=0. While for large value of q_s, no appreciable in ε

was found. This suggests that the stability of the ELM depends on the surfactant concentration, and also there is a "*critical concentration*" of q_s, found to be 5.8×10^{-9} kmol/m^2. In conclusion, a stable ELM is formed by about 1.6 layers of the surfactant adsorbed at the interface, provided that the effective constituent in Span80 is of 80%.

For $(W/O)/W$-dispersion systems with various ϕ and Φ, plotting ε against q_s in the same way as Fig. 3. 25, we also obtained a linear relation. In the case of larger ϕ and Φ, the slope of the line becomes steeper and the ELM is then more stable. The effects of ϕ and Φ

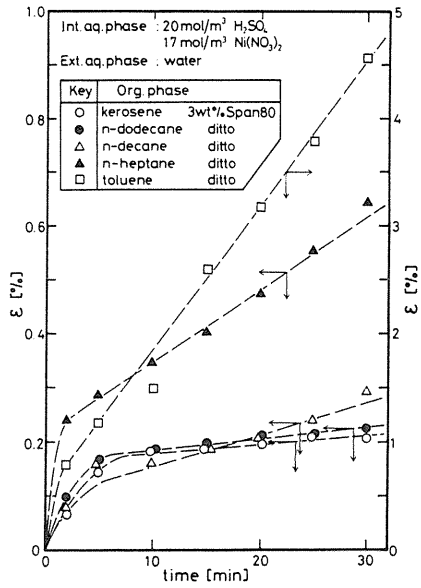

Fig. 3. 24. Membrane stabilities of (W/O) droplets consisting of various organic solvents in $(W/O)/W$ emulsions.

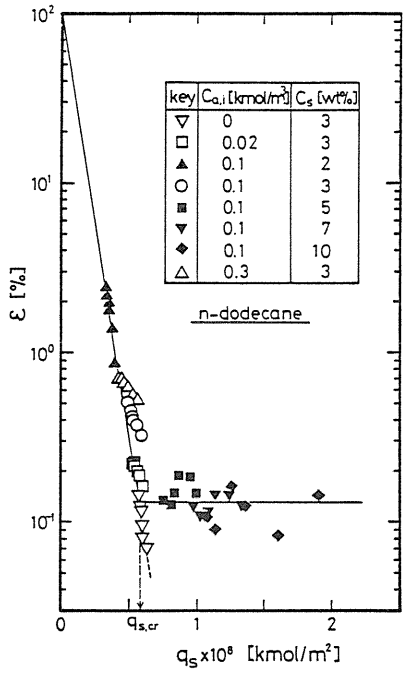

Fig. 3. 25. Effect of concentrations of the surfactant and of the acid in the inner aqueous phase on the breakdown ratio for *n*-dodecane system.

may be attributed to an increase in the apparent viscosities of (W/O)- and $(W/O)/W$-emulsion due to the shear thickenning for non-Newtonian fluid. Furthermore, the linear relation between q_s and ε was obtained for the respective organic solvents. Fig. 3. 26 shows a plot of the slope against the solvent viscosity, μ_o. No significant deviation from a line is observed for the data points with exception of the toluene system. This result suggests that in a series of hydrocarbons, the stability of ELMs could be correlated with the viscosity of the solvent.

3. 3. 5. Water Permeation Coefficient and Water Entrainment in (W/O)/W Dispersions[51,52]

Water permeation coefficient across the ELM, P_o, was evaluated from the following equation[53] based on the change in $V_i/V_{i,0}$:

$$P_o = (dV_i/dt)/[A\nu g(C_i - C_e)V_m] \tag{54}$$

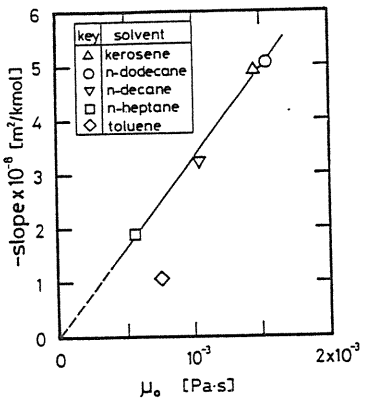

Fig. 3. 26. Effect of viscosity of the organic solvent on a stability of ELM for various organic solvent.

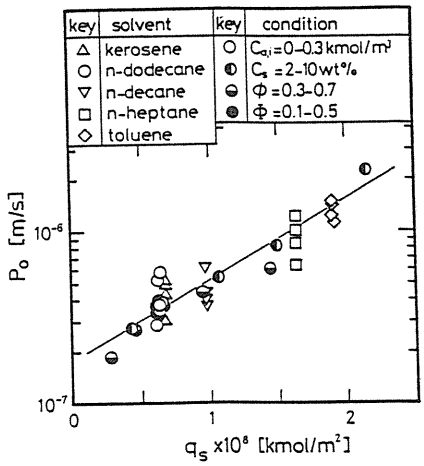

Fig. 3. 27. Correlation of water permeation coefficient with the surfactant concentration at interface for various organic solvent systems.

where dV_i/dt is the volume flux of water across the membrane, g the osmotic coefficient and V_m the partial molar volume of water. The volume of the water transported is given as the sum of the amounts due to the permeation and entrainment. We here assumed that the former is expressed by Eq. (54), whereas the latter is caused only by the processes of dispersing and coalescing of (W/O) droplets before attaining a state of equilibrium dispersion. The entrainment is considered to end within the first 5 *min*, as was shown in Fig. 3. 22. Thus, the interfacial area of (W/O) drops for the water permeation, A, was obtained from the Sauter mean diameter at 5 min after contacting (W/O) emulsion with the external aqueous phase.

To evaluate the P_o value, $V_i/V_{i,o}$ was repeatedly calculated by solving the difference equation of Eq. (54) with an assumed value of P_o. The values of P_o thus obtained are plotted in Fig. 3. 27 against q_s. The effects of operating conditions (C_s, ϕ, Φ) and organic solvents on P_o can be quantitatively explained in terms of q_s. Consequently, an increase in the surfactant concentration at the interface enhances the water permeation through the ELM, though the permeation mechanism is obscure. Fig. 3. 28 shows the effect of C_s on the solubility of water into the kerosene solution. The solubility increases with C_s; however, the solubilized water is not as much as possible to explain the increase in P_o or V_i under osmotic conditions. This implies that the mechanism based on the solubilization has a weak theoretical ground. A potential for water permeation can be regarded as being a pressure difference, and therefore, water seems to penetrate through a hole formed in the ultra-thin layer on the external surface of (W/O) droplet.

Fig. 3. 29 shows the volume of water entrained in the (W/O)-emulsion as a plot of $V_{ent}/V_{i,o}$ versus q_s, implying that for *n*-dodecane systems the increase in q_s also brings about an effect on the entrainment due to emulsification (solid line). The secondary emulsification, however, could take place for the duration of initial dispersion of the (W/O)-emulsion, then attaining a steady state in dynamic equilibrium with the breakdown of the (W/O) drops emulsified the external phase. Moreover, (W/O)-emulsions consisting of *n*-heptane or

toluene have less mechanical strength, as mentioned above. From the discussion, it can be concluded that the water entrainment in such a (*W/O*)/*W*-emulsion system is reduced apparently at the same q_s value, compared with the result for *n*-dodecane system giving a stable ELM.

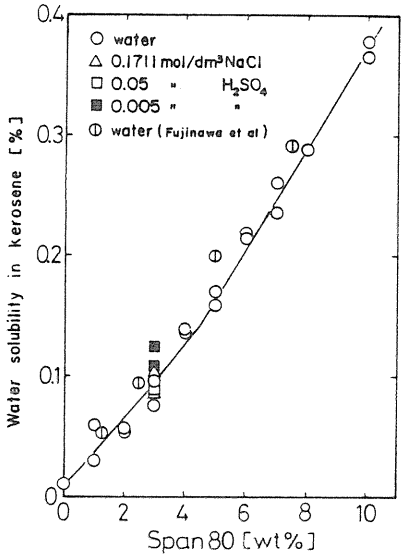

Fig. 3. 28. Effect of content of Span80 on water solubility in kerosene.

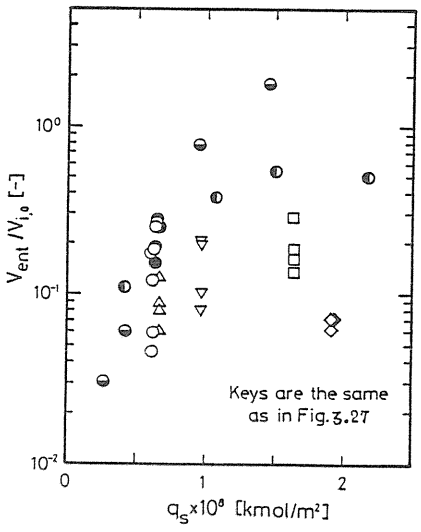

Fig. 3. 29. Effect of the surfactant concentration at the interface on the water entrainment in various (*W/O*)-emulsion drops.

4. Separation of Metal Ions Using Supported Liquid Membranes

4. 1. Ion Transport through an SLM Containing Crown Ether[54]

Transport of ions across a liquid membrane was studied by using a cyclic polyether dibenzo-18-crown-6 ($C_{20}H_{24}O_6$, molecular weight 360) as the mobile carrier for alkali metal ions. The liquid membrane consisted of the polyether in tetrachlorethane, held in a piece of *Millipore* filter (d_p=10.0 μm, δ=125 ± 15 μm, ε=0.68), being sandwiched between two sheets of *Cellophane* in a modified diaphragm cell.

The initial flux of cation across the SLM was evaluated from the overall flux, N_O, across the sandwiched membrane as follow:

$$N_O = V_2 (dC_2/dt) = K_O S (C_1 - C_2) \tag{55}$$

where, V_2 is the volume of upper compartment of the cell; C the concentration of alkali ion; S the total effective cross-sectional area; the subscripts *1* and *2* represent the lower and upper compartments of the cell.

We here assumed that the dominant solute-carrier reaction involves ion-pair formation: the cation (I^+) and anion (B^-) could dissolve in the membrane and react to form a complex with the polyether (C). For multi-cations system, each cationic species (i^+) reacts with B^- and C:

$$i^+ + B^- + C \leftrightarrows (iBC) \tag{56}$$

When considering the partition coefficients of the ion pair between aqueous phase and the membrane solvent, ($k_i = C^*_{iB}/C_i\ C_B$), and the equilibria in the membrane phase, ($k_i = C_{iBC}/k_i\ C_B\ C_c$), the permeation flux of i-species can be expressed by

$$J_i = \frac{D_i k_i}{\ell}(C_{i1}\ C_{B1} - C_{i2}\ C_{B2}) + \frac{D_{iBC}\ k_i\ K_i}{\ell} \times \left[\left(\frac{C_{i1}\ C_{B1}\ C_{T1}}{1 + \sum_{i=1}^{n} k_i\ K_i\ C_{1i}\ C_{B1}}\right) - \left(\frac{C_{i2}\ C_{B2}\ C_{T2}}{1 + \sum_{i=1}^{n} k_i\ K_i\ C_{i2}\ C_{B2}}\right)\right] \tag{57}$$

where

$$C_T = C_C + \sum_{i=1}^{n} C_{iBC} \tag{58}$$

The first term on the right-hand side of Eq. (57) represents the ordinary diffusion of ion pairs, and the second represents carrier-mediated diffusion.

The overall transport coefficient can be given by

$$1/K_O S = (\ell/S)_c(1/D_i) + (\ell/S)_m(1/Fm\ D_{iBC}) + (\ell/S)_c\,(1/D_i) \tag{59}$$

provided that the carrier enhances the permeation flux by the facilitation factor, F, where the $(\ell/S)_m$ and $(\ell/S)_c$ are the cell constants for SLM and for the *cellophane* membrane, respectively. From Eqs. (57) and (59), we can obtain the permeation flux of i-species through the SLM by considering the initial conditions: $C_1 = C_0$ and $C_2 = 0$ at $t = 0$.

$$N_{i,\,t=0} = (N_O)_{t=0}/[C_0 - 2(N_O)_{t=0}(\ell/S)_c\,(1/D_i)] \tag{60}$$

Fig. 4. 1 shows the effect of the product of C_i and C_B on the value of $(N_i)_{t=0}$ for the single salt solutions at $C_T = 0.1\ M$, indicating that the flux of each cation can be expressed by Eq. (57). This suggests that the polyether has the selectivity for the formation of each complex with alkali metal ion. Also, Fig. 4. 2 illustrates the effect of the crown concentration on the flux of K^+ in the presence of Na^+, wherein the intercept $N_{K,t=0}$ represent the flux due to the ordinary diffusion.

For multi-cations system, the selectivity to permeation of i- to j-sepecies is defined as the flux ratio based on Eq. (57).

$$S_{ij} = J_i/J_j = \frac{D_{iBC}}{D_{jBC}} \cdot \alpha_{ij} \cdot \frac{(C_{i0}/C_{B0})}{(C_{j0}/C_{B0})} \tag{61}$$

where $\alpha_{ij} = k_iK_i/k_jK_j$ and the first term on the right hand side of Eq. (57) was neglected. Fig. 4. 3 shows a plot of $(N_i)_{t=0}$ versus C_iC_B for the results obtained for the mixed salt systems given in Table 4. 1. Here, the values of S_{ij} obtained from the figure are plotted in Fig. 4. 4 against the concentration ratio of cation, wherein the slope of each line corresponds to α_{ij}. Thus we can calculate K_i/K_j with an assumption that $k_i/k_j \simeq 1$, and then the values are given in Table 4. 2, together with literature values[55] for various organic solvents. The difference in the K_i/K_j-values among the organic solvents may be attributed to the dielectric constant. Further experiment was made on the membrane conductance; we then obtained the values of $S_{K\text{-}Li}$=4.9, $S_{Na\text{-}Li}$=2.1 and $S_{K\text{-}Na}$=2.3 as the selectivity.

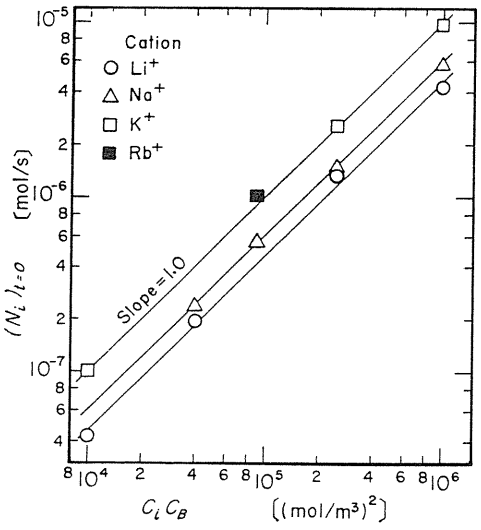

Fig. 4. 1. Effect of the product of C_i and C_B on $(N_i)_{t=0}$ for single salt (C_T=0.1 M).

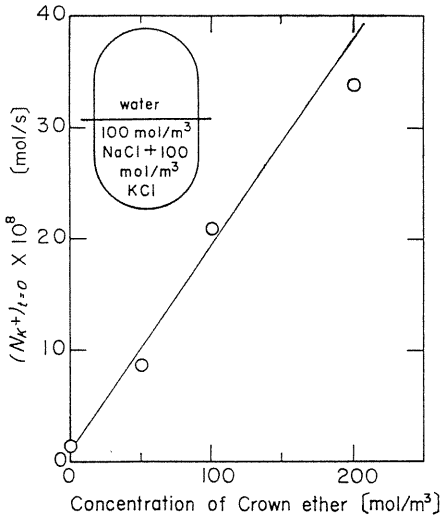

Fig. 4. 2. Effect of carrier concentration on cation transport.

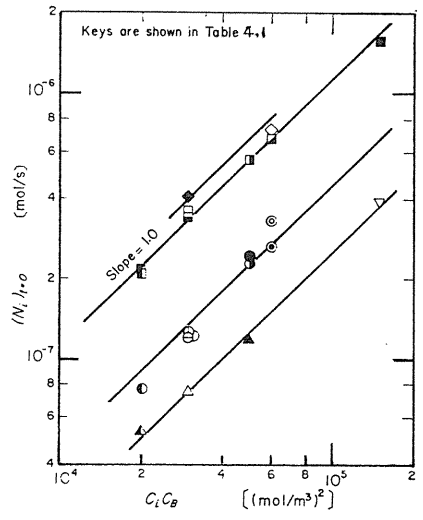

Fig. 4. 3. Effect of the product of C_i and C_B on $(N_i)_{t=0}$ for mixed salt. (C_T=0.1 M).

Table 4. 1. Concentration of salts used for multi-cations transport across SLM with a crown ether.

System	Salt concentration [mol/m³]				Key mark			
	LiCl	NaCl	KCl	RbCl	Li^+	Na^+	K^+	Rb^+
1	100		100		△		□	
2		100	100			◐	◪	
3		100	200			◑	◪	
4		100		200		⊖		◇
5		200	100			◉	▬	
6		200		100		◎		◆
7	100	100	100		△	○	□	
8	100	100	300		▲	●	■	
9	300	100	100		▽	◑	◨	

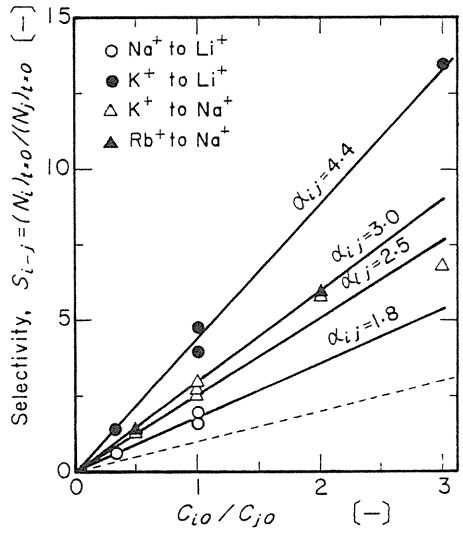

Fig. 4. 4. Effect of C_{i0}/C_{j0} on selectivity.

Table 4. 2. Selectivities of dibenzo-18-crown-6 in various organic solvents for alkali metal ions.

Organic solvent	K_{K^+}/K_{Li^+}	K_{Na^+}/K_{Li^+}	K_{K^+}/K_{Na^+}	K_{Rb^+}/K_{Na^+}	K_{Cs^+}/K_{Na^+}
Dimethyl sulfoxide*			1.276	1.151	1.008
N, *N*-dimethyl formamide*	3.310	2.077	1.594	1.520	1.375
Propylene carbonate*	64.647	3.982	16.235	0.768	0.479
Tetrachloroethane**	4.4	1.8	2.5	3.0	

* Literature value (55) ** This work ($K_iK_i/K_jK_j \simeq K_i/K_j$)

4. 2. *Enrichment of Cobalt in a Multi Hollow-fibers SLM Module*[17]

As described in **3. 2. 2**, it was found that a stable *CR*-SLM operation can be attained in the multi-HFs type SLM in crossflow mode. Thus, using the module shown in Fig. 3. 11b, which allows a larger contact area per unit volume, we examined the enrichment of metal ion by uphill transport from a dilute aqueous-feed stream to dense receiving solution against the concentration gradient. In the present experiment, Co^{2+} was transferred across the *CR*-SLM with *PC-88A* in n-heptane from the nitrate solution of 9.2×10^{-3} *M* to nitric acid solution (0.01 *M*) containing Co^{2+} ranged from 0 to 1 *M*. As expected from the extraction equilibrium (see **2. 3. 3**), both permeation fluxes of Co^{2+} and H^+ were satisfied with the relation of $J_{Co}=-J_{H/2}$.

Fig. 4. 5 shows the effect of Co^{2+} concentration in the receiving phase, $[Co^{2+}]_{s,b}$, on J_{Co}, wherein a solid line repesents the calculated value with an assumption of the equilibrium process, involving the diffusional resistances through the two aqueous boundary films and through the membrane layer. A good agreement of the calculation with the observed value indicates that both forward and backward extractions proceed at a faster rate than those for the diffusion processes mentioned above. Furthermore, the permeation of Co^{2+} across the *CR*-SLM proceeds at a constant rate even for the uphill transport against the concentration gradient, whereby the ion can be pumped up to a concentration near the saturation. However, the enrichment ratio was no more than about 100 even at the maximum value, because of the comparatively high concentration of Co^{2+} in the aqueous feed.

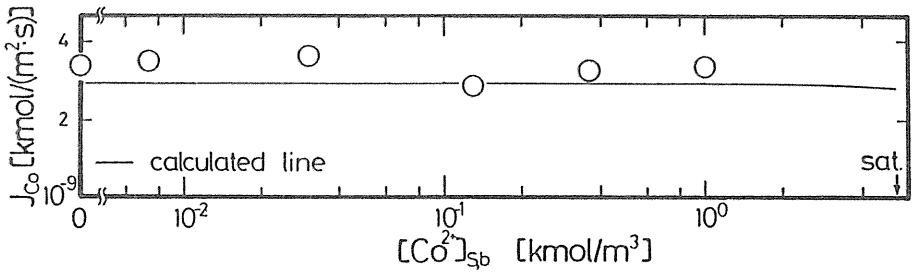

Fig. 4. 5. Effect of cobalt concentration in the strip liquor, $[Co^{2+}]_{s.b}$, on the uphill transport. *Sat.* presents the saturation of $Co(NO_3)_2$. Feed: $[Co^{2+}] = 9.2\times10\,cm^{-3}M$, *pH*4.7, flow rate = 3 cm^3/s. Strip liquor: 0.01 *M*-HNO_3, U_s = 3 cm/s. Membrane liquid: 0.08 *M*-EHPNA in *n*-heptane.

4. 3. *Fractional Separation of Metal Ions in One-Stage CR-SLM Operation*[17]

We here consider an SLM-separation of metals in a ternary solution. If a third metal in the solution can be extracted on the feed side on the SLM but not be stripped on the recovery side; then the respective metals may be fractionally separated in a one-stage operation: the permeate (downstream), extract (membrane solution) and raffinate (upstream). Thus, one can expect that the third metal is carried over with the membrane-liquid flow by use of the present *CR*-SLM. This view was demonstrated on the one-stage separation of divalent metals from the ternary solution of Ni(II)-Co(II)-Zn(II), as in Fig. 4. 6.

Typical results for a preliminary test in a semi-batch operation are shown in Fig. 4. 7 as the time courses of the concentrations of Ni, Co and Zn in aqueous solution on the upstream side, C_F, and in buffered strip solution, C_S. Both cations of Co and Zn are taken up in the

membrane phase by the extraction on the feed side, and then only the extracted Co is released in the strip liquor, whereas a little Ni is extracted in the membrane phase. This suggests a possibility of the fractional separation of multi-cations in the *CR*-SLM operation; thus, further experiments were made on the continuous separation. In the present situation,

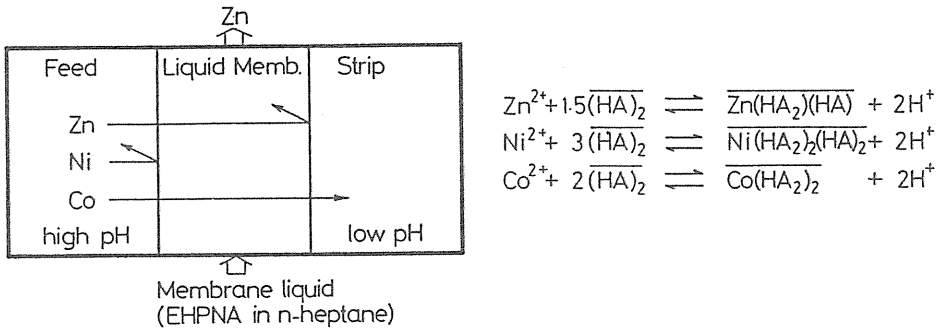

Fig. 4. 6. Principle of fractional separation of ternary metal solution by using a *CR*-SLM.

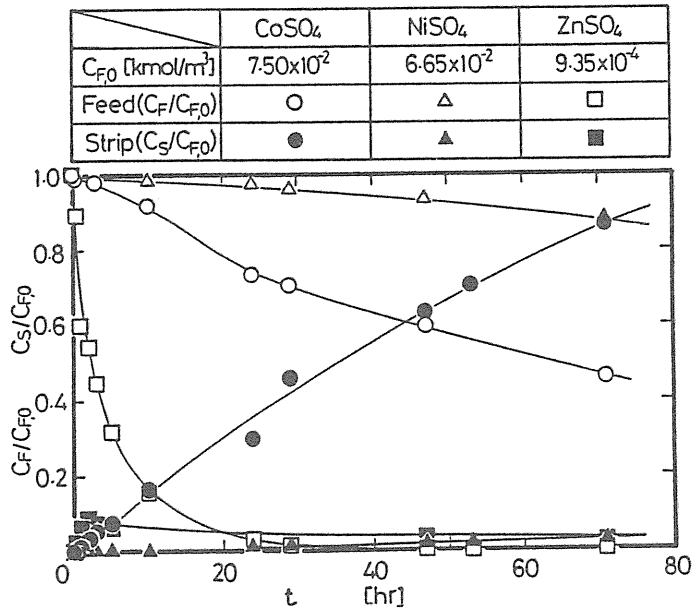

Fig. 4. 7. Time courses of the concentrations of Ni, Co, and Zn in the feed and strip solutions in a semi-batch operation. Feed side: *pH* 3.8–4.1 (Acetate buffer), $U_F = 4$ cm/s, $V_F = 200$ cm^3. Strip side: *pH* 1.9–2.2 under controlling on *pH*-stat with 0.1 *N*-H_2SO_4, $U_S = 3$ cm/s, $V_S = 100$ cm^3.

we considered two fluxes for each cation in the feed: the permeation flux across the membrane, J, and "*carry-over*" flux with the membrane flow, $\bar{J}$. The latter is an apparent flux based on the area for the extraction on the feed side; the total flux for the extraction of metal in the SLM from the aqueous feed can be expressed by $J+\bar{J}$, corresponding to the uptake in the membrane phase.

Fig. 4. 8 shows the effect of flow rate of the membrane liquid, Q_{oil}, on both the fluxes of J and $\bar{J}$ for the metals. With increasing Q_{oil}, the J_{Zn} is lowered; however, the flow effect on the uptake of Co(II) is of little significance in addition to an increase in the carry-over of Co(II), $\bar{J}_{Co}$. It can be expected that an increase in $\bar{J}_{Zn}$ gives rise to higher separation factor of Zn(II) to Co(II), and the strip liquor pH may play a major role in controlling J_{Zn} and $\bar{J}_{Zn}$.

The effect of proton concentration in the strip liquor, $[H^+]_{s,b}$, on the values of J and $\bar{J}$ is illustrated in Fig. 4. 9, wherein a remarkable effect of $[H^+]$ on J_{Zn} is found in contrast to J_{Co} as well as J_{Ni}, though the separation factor of Co(II) to Ni(II), $S_{Co/Ni}$ is more than 30 ~ 40. Such a smaller separation factor may be attributed to the lower $[H^+]_i$ at both interfaces on the upstream and downstream sides. For the binary solution of Ni and Co, we obtained a maximum value of $S_{Co/Ni}$ of *ca.*1300 for a buffered feed; however, when the buffer action was weak, the increase in $[H^+]_i$ caused a drastic decline in the S value, depending on the extraction equilibria. (See Fig. 2. 22).

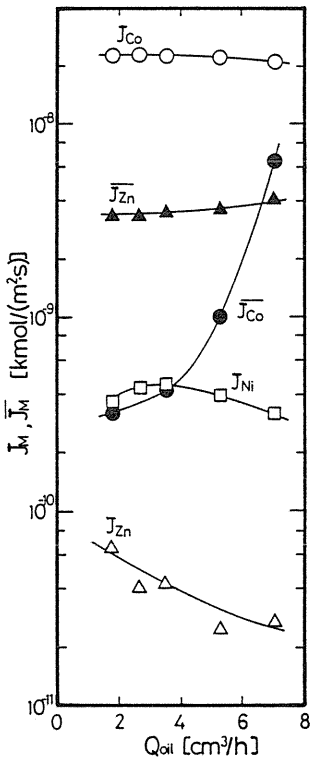

Fig. 4. 8. Effect of membrane liquid flow rate, Q_{oil}, on the permeation flux and the uptake in the membrane phase. Feed: $[Ni^{2+}] = [Co^{2+}] = 0.01\,M$, $[Zn^{2+}] = 4\times10^{-4}\,M$, *pH* 3.9 (Acetate buffer), $U_F = 4.4$ cm/s. Strip liquor: *pH* 2.7, $U_S = 3$ cm/s.

Fig. 4. 10 shows the effect of the concentration of Zn(II) in the presence of Co(II) in the aqueous feed, indicating that the permeation flux of Zn(II) decreased dramatically with increasing $[Zn]_{F,b}$. To obtain the maximum separation in the present *CR*-SLM, it is crucial to suppress the permeation of Zn(II) across the membrane. This can be attained by controlling the strip liquor *pH* at an optimum value; however, the distribution ratio of Zn(II) in the present system is larger than that of Co(II) by three or four orders of magnitude. Therefore, the high concentration of Zn(II) in the feed is responsible for a significant decline of the *pH* at the interface, resulting in a lower uptake of Co(II) by the extraction. Consequently, in this fractional separation of the three cations, it is advisable for the aqueous feed with the concentration of Zn(II) less than one-tenth of that of Co(II).

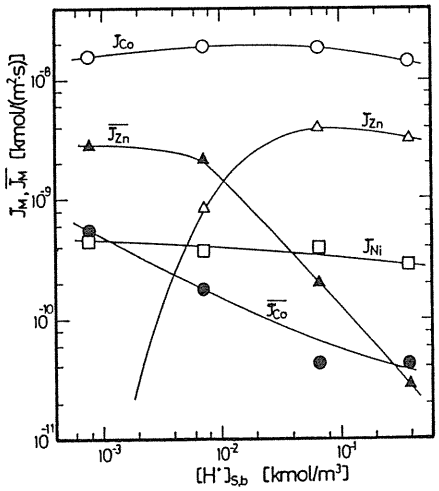

Fig. 4. 9. Effect of proton concentration in the strip liquor on the fractional separation. Feed: $[Ni^{2+}] = [Co^{2+}] = 0.01\,M$, $[Zn^{2+}] = 3.7\times10^{-4}\,M$, *pH* 3.9 (Acetate buffer), $U_F = 4.4$ cm/s. Strip liquor: $U_S = 3$ cm/s. Memb. liq: $Q_{oil} = 1.76$ cm^3/hr.

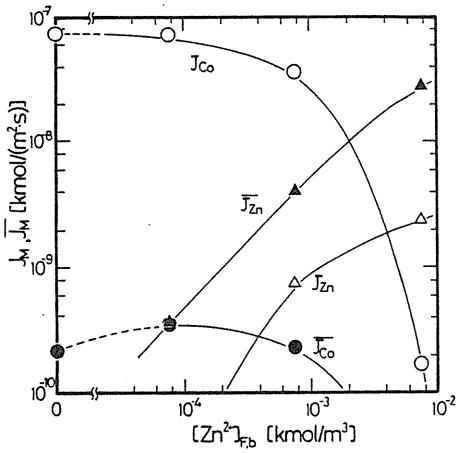

Fig. 4. 10. Effect of zinc concentration in the binary feed of Co^{2+} and Zn^{2+} on the selective separation. Feed: $[Co^{2+}] = 9.1\times10^{-3}\,M$, *pH* 5.6 (Acetate buffer), $U_F = 4.5$ cm/s. Strip liquor: *pH* 2.8, $U_S = 3$ cm/s. Memb. liq.: $Q_{oil} = 1.7$ cm^3/hr.

4. 4. Recovery of Cr(VI) from Sulfuric Acid Media Using a Flat Types SLM in Continuous Regenerating Mode[56]

To maintain the stability of SLMs, the mixed flow mode was confirmed to be useful to flat-type membrane modules, as described in **3. 2. 1**. In this section the recovery of Cr(VI) was studied by using a multi-layer type of an SLM with a nitrobenzene solution of *3-(4*-pyridyl)-*1,5*-diphenyl pentane (*PDPP*). The SLM device, in which several flat sheets of *FP-045* membrane were stratified alternatively with *PTFE* spacers (1 mm in thickness), has a flow channel of 3 mm width and 58 cm effective length per a sheet of the membrane. Aqueous feed was a sulfuric acid solution of $K_2Cr_2O_7$, the receiving phase being an ammoniacal solution (*CaseI*) and that with $K_2Cr_2O_7$ (*CaseII*). In the experimental runs, the feed flowed through the channel in a once-through mode, whereas the recovery solution was recirculated through the other channel *via* a reservoir, then a small amount of the membrane liquid being supplied at the inlet of the device.

Fig. 4. 11 shows the variation of the fractional residue of Cr(VI), *1-R*, in the effluent from the feed channel in the device with a sheet of SLM with and without the membrane liquid flow on the recovery side, where *R* represents the recovery fraction of Cr(VI), given by $1\text{-}C_{F,out}/C_{F,in}$. When the membrane liquid was forced to flow with the recovery solution at a superficial velocity, $U_{R,or}$, of 0.01 cm/s, the recovery fraction approaches a constant value within a short duration. Furthermore, the *R* value increased with increasing number of the membrane in the device; thus, we used the SLM module consisting of seven sheets of the membrane in the following experiments.

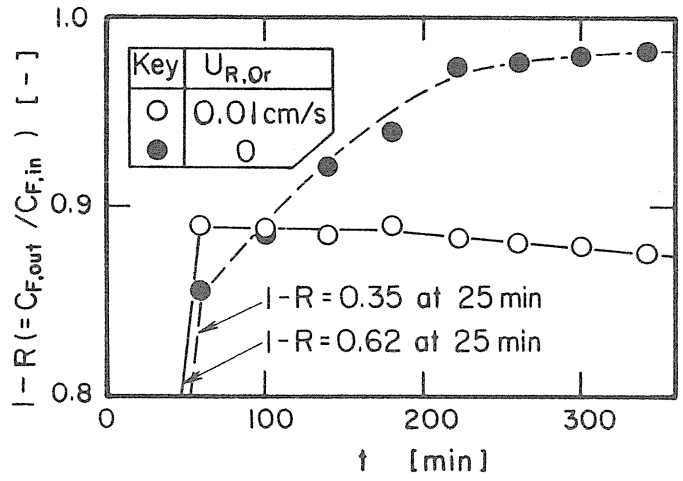

Fig. 4. 11. Residuary fraction of Cr(VI) in feed solution for experiments with and without membrane solution flowing with recovery solution. (X = 0.58 m, U_F = 0.40 cm/s, $C_{F,in}$ = 4.7 mM, $pH_{F,in}$ = 1.6, U_R = 0.62 cm/s, C_R = 0, $pH_{R,in}$ = 8.8).

In a practical situation metal ion concentration in the receiving phase is higher than that in the feed solution, whereby the permeation of the metal across SLM proceeds against the concentration gradient as an uphill transport. We here examined the recovery of Cr(VI) from the aqueous feed of 2.1 mM to the receiving phase of 60 mM: *CaseII*. The results are shown in Fig. 4. 12 against the feed velocity, U_F, together with those obtained for *CaseI*. A high recovering efficiency was attained by use of the multilayer SLM. However, when using the receiving solution containing only ammonia (*CaseI*), Cr(VI)-*PDPP* complex has accumulated within the SLM (See **2. 3. 2**), and then the R-value decreases with time as can be seen in Fig. 4. 11. On the other hand, the addition of Cr(VI) to the receiving solution gave rise to an improvement of the recovering efficiency in *CaseI*. Also it was found that the experimental results are in good agreement with the calculated values (dashed line in Fig. 4. 12), taken into consideration the interfacial reaction given by Eq. (22) on both sides of the SLM as well as the diffusion resistances through the aqueous boundary film and SLM. In this calculation, we used the diffusion coefficients of Cr(VI) and H^+ by the Vinograd and McBain equation: D_{Cr}=1.4×10^{-9} m^2/s and D_H=2.2×10^{-9} m^2/s. The membrane transfer coefficient was evaluated from k_m=0.22 $D\varepsilon/\delta$ (see Fig. 2. 9) with an assumption of $(PDPP)_3(H_2CrO_4)_2$ as the Cr(VI)- complex (see **2. 3. 2**).

Chromium has been used extensively as corrosion inhibitors as well in electroplating; thus, further experiment was made on the effect of coexisting heavy metal ions in a viewpoint of the recovery of Cr(VI) from such industrial wastewaters. From the examination of solvent effect as the diluent of *PDPP*, benzene has proved to be favorable to the membrane solvent in the present SLM separation: lower permeation fluxes for both H_2SO_4 and NH_3. Fig. 4. 13 shows the effect of coexistence of Fe(III), Zn(II) and Cu(II) in an aqueous Cr(VI) feed on the respective metal recoveries (R and R_Y). No significant effect is observed in the presence of Cu(II) or Fe(III), whereas Zn(II) had a remarkable effect with an increase in its concentration and interfered with the permeation of Cr(VI) through the SLM. In conclusion, Cr(VI)

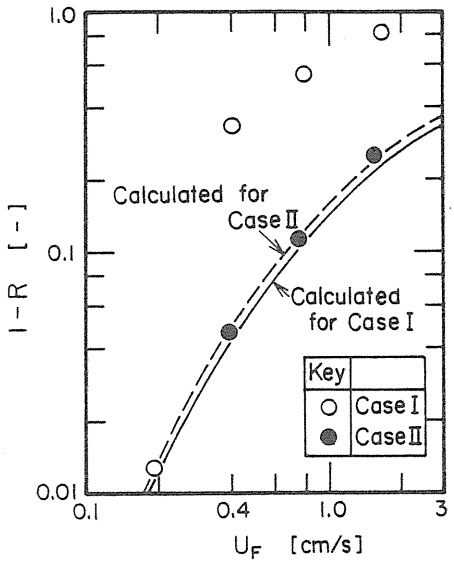

Fig. 4. 12. Effect of U_F on *1-R* for $X =$ 4.08 m, $pH_{R,in} = 8.8$, $U_R =$ 0.62 cm/s and $U_{R,Or} =$ 0.01 cm/s. *Case I:* $C_{F,in} =$ 4.7 *mM*, $pH_{F,in} = 1.6$ and $C_R = 0$, and *Case II*: $C_{F,in} =$ 2.1 *mM*, $pH_{F,in} = 2.0$ and $C_R = 60$ *mM*.

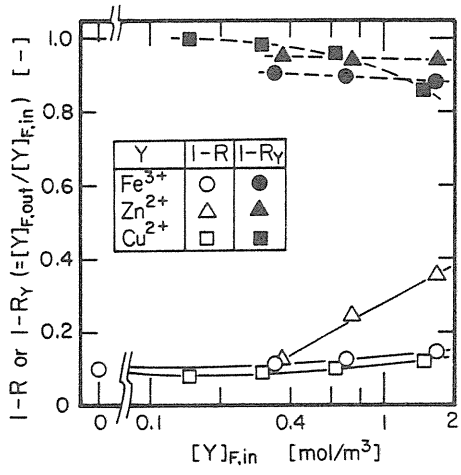

Fig. 4. 13. Effects of metal ions coexisting with Cr(VI) on *1-R*.

can be preferably recovered from the aqueous feed containing these heavy metal ions.

5. Conclusion

In this article we provided a survey of the results of our investigations on liquid membranes, especially with a view to recovering and concentrating metal ions from these dilute aqueous solutions. The primary application areas where the separations of carrier-mediated liquid membrane systems show potential are in the removal of toxic species from environmental samples, analytical separation and/or concentration procedure, and industrial separations. Industrially, highly selective separation processes include gas separation, valuable metal recovery and organic molecule separations, which could use molecular recognition technology coupled with appropriate membrane system. However, only a few applications for separation using liquid membranes are practically being used at present time. A variety of problems remain to be solved. Among them, development of the type of module is a prime factor in assuring the possible operating stability of the liquid membrane used; some of the countermoves have been considered.

In conclusion, an understanding of all system parameters which affect membrane

performance is necessary to design a stable liquid membrane as well as to perform the desired separation. In special, synthesis of carrier and emulsifying agents having other excellent capabilities and the development of microporous polymeric supports having uniform pore size are eagerly awaited.

References

1) W.J.V.Osterhout; Some Models of Protoplasmic Surface, *Cold Sparing Harbor Symp. Quant. Biol.*, **8**, 51 (1940).
2) P.F.Scholander; Oxygen Transport Through Hemoglobin Solution, *Science*, **131**, 585 (1960).
3) W.J.Ward and W.L.Robb; Carbon Dioxide-Oxygen Separation: Facilitated Transport of Carbon Dioxide Across a Liquid Film, *Science*, **156**, 1481 (1967).
4) N.N.Li and N.J.Somerset; Separating Hydrocabons with Liquid Membrames, *U.S. Patent* 3,410,794 (1968).
5) H.Takeuchi; Some Problems in Separation Processes Using Liquid Membranes, *Chemical Engineering*, **33**, 853 (1988).
6) K.Takahashi, M.Kato, K.Hirayama & H.Takeuchi: Simultaneous Determination of Water and Oil-Phase Transfer Coefficients in Liquid-Liquid Extraction, *Kagaku Kogaku Ronbunshu*, **11**, 110 (1985).
7) K.Takahashi, M.Nakano & H.Takeuchi; Mass Transfer Coefficients in a Flat Type Supported Liquid Membrane, *ibid.*, **13**, 256 (1987).
8) W.M.Kays and M.E. Crawford; "*Convective Heat and Mass Transfer*", **2nd ed.**(1980), p.139, McGraw Hill, New York.
9) H.Takeuchi, K.Takahashi & M.Nakano; Mass Transfer in Single Oil-Containing Microporous Hollow-Fiber Contactors, *Ind. & Eng. Chem. Research*, **29**, 1471 (1990).
10) K.G.Darrall & G. Oldhan; The Diffusion Coefficients of the Triiodide Ion in Aqueous Solutions, *J. Chem. Soc., A*, 2584 (1968).
11) M.C.Yang & E.L.Cussler; Designing Hollow-Fiber Contactors. *AIChE J.*, **32**, 1910 (1986).
12) M.A.Leveque; Les Lois de la Transmission de Chaleur par Convection, *Ann. Mines Rec. Mem. L'Explotas. Mines*, **13**, 201 (1928).
13) R.Prasad & K.K.Sirkar; Dispersion-Free Solvent Extraction with Microporous Hollow-Fiber Modules., *AIChE J.*, **34**, 177 (1988).
14) T.H.Chilton & A.P.Colburn; Mass Transfer (Absorption) Coefficients, Prediction from Data on Heat Transfer and Fluid Friction, *Ind. Eng. Chem.*, **26**, 1183 (1934).
15) L.Dahuron & E.L.Cussler; Protein Extractions with Hollow Fibers, *AIChE J.*, **34**, 130 (1988).
16) E.L.Cussler; "*Diffusion: Mass Transfer in Fluid System*", Chapter **7**, Cambridge Univ. Press (1984).
17) H.Takeuchi, K.Takahashi & M.Nakano: Separation of Heavy Metals from Aqueous Solutions by Hollow-Fiber Type Supported Liquid Membranes in a Continuous Regenerating Mode, *WATER TREATMENT*, **5**, 222 (1990).
18) M.N.Pons; Monte-Carlo Model of Microporous Plane Membranes, *Chem. Eng. J.*, **35**, 201 (1987).
19) K.Onda, H.Takeuchi & M.Fujine; Study of Mass Transfer between Phases by Diaphragm Cell — Physical Absorption of CO_2 into Water or Aqueous Electrolyte Solutions, *J. Chem. Eng. J.*, **8**, 25 (1975).
20) K.Onda, H.Takeuchi & M.Fujine; Study of Mass Transfer between Phases by a Diaphragm Cell — Alkaline Hydrolysis of Esters in Aqueous NaOH Solution, *ibid.*, **8**, 30 (1975).
21) H.Takeuchi, M.Fujine & K.Onda; Simultaneous Determination of Difffusion Coefficient and Solubilities of Gas in Liquid by a Diaphragm Cell, *ibid.*, **8**, 252 (1975).
22) M.Takahashi & H.Takeuchi; Diffusion Coefficients and Solubilities of Carbon Dioxide in Binary

Mixed Solvents, *J. Chem. Eng. Data*, **27**, 328 (1982).
23) D.M.Malone & J.L.Anderson; Diffusional Boundary-Layer Resistance for Membranes with Low Porosity, *AIChE J.*, **23**, 177 (1977).
24) K.Takahashi, H.Kamiya & H.Takeuchi; Extraction of Copper by LIX65N in a Vessel and Multi-stage Column under Stirred Conditions, *Solvent Extr. & Ion Exchange*, **1**, 311 (1983).
25) K.Takahashi & H.Takeuchi: Rates of Copper Extraction by LIX65N, *Kagaku Kogaku Ronbunshu*, **10**, 409 (1984).
26) K.Takahashi & H.Takeuchi; Stripping Rates of Copper for LIX65N-Copper System. *ibid.*, **10**, 543 (1984).
27) K.Takahashi & H.Takeuchi; Copper Extraction by LIX65N in Liquid-Liquid Dispersion System, *ibid.*, **11**, 349 (1985).
28) K.Takahashi & H.Takeuchi; Behavior of Interfacial Tension during Copper Extraction by LIX65N, *J. Chem. Eng. Jpn.*, **19**, 161 (1986).
29) K.Takahashi, F.Ohtsubo & H.Takeuchi; Extraction of Copper by (W/O)/W Emulsion Type Liquid Membrane Containing LIX65N, *Kagaku Kogaku Ronbunshu*, **9**, 409 (1983).
30) K.Takahashi, K.Hirayama & H.Takeuchi; Solvent Extraction of Chromium(VI) by 3-(4-pyridyl)-1,5-Diphenyl Pentane, *Solv. Extr. & Ion Exchange*, **5**, 393 (1987).
31) S.Uchida, K.Takahashi & H.Takeuchi; Extraction Equilibria of Lanthanum, Copper and Cobalt by 2-Ethylhexyl Phosphonic Acid Mono (2-Ethyl hexyl) Ester, *Proc. of Symp. on Solv. Ext. of Metals* (Hamamatsu), p.13 (1981).
32) M.Tanaka; "*Yobaichushutu no Kakagaku*", 1-st ed. Nankoudo (1979).
33) M.Takahashi & H.Takeuchi; Solvent Extraction of Cadmium by Di(2-ethylhexyl)Phosphoric Acid, *Kagaku Kogaku Ronbunshu*, **11**, 628 (1985).
34) M.Takahashi, A.Uemura & H.Takeuchi; Stripping Rates of Cadmium for D2EHPA-Cd System, *ibid.*, **13**, 127 (1987).
35) M.Takahashi, F.Kanamori, T.Kakiuchi & H.Takeuchi; Solvent Extraction of Gallium from Aqueous Hydrochloric Acid Solutions by an Organophosphorous Monoester in n-Heptane, *ibid.*, **15**, 1006 (1989).
36) K.Iio, K.Takahashi & H.Takeuchi; Solvent Extraction of Titanium(IV) from Nitric Acid Solution by Di(2-Ethyl)Phosphoric Acid, *Solv. Ext. & Ion Exchn.* **9**, 27 (1991).
37) M.Takahashi, T.Ohta, Y.Katayama & H.Takeuchi: Permeation Rates of Cadmium through a Supported Liquid Membrane Containing D2EHPA, *Kagaku Kogaku Ronbunshu*, **14**, 549 (1988).
38) H.Takeuchi, K.Takahashi & W.Goto; Some Observations on the Stability of Supported Liquid Membranes, *J. Membrane Sci.*, **34**, 19 (1987).
39) H.Takeuchi & M.Nakano; Progressive Wetting of Supported Liquid Membranes by Aqueous Solution, *ibid.*, **42**, 183 (1989).
40) M.Nakano, K.Takahashi & H.Takeuchi; Characterization of Water in n-Heptane Solutions of Nickel (II) and Cobalt (II)-Organophosphorous Acid Complexes, *Proc. of Symp. on Solvent Extr. 1987* (Osaka), p.81 (1987).
41) H.Takeuchi, K.Takahashi & M.Nakano: Interfacial Tension during Extraction of Nickel and Cobalt by Organophosphorous Esters, *Kagaku Kogaku Ronbunshu*, **16**, 184 (1990).
42) B.Kim & P.Harriott; Critical Entry Pressure for Liquids in Hydrophobic Membranes, *J. Colloid and Interface Sci.*, **115**, 1 (1987).
43) K.Takahashi & H.Takeuchi; Transport of Copper through a Supported Liquid Membrane, *J. Chem. Eng. Jpn.*, **18**, 205 (1985).
44) M.Nakano, K.Takahashi & H.Takeuchi; A Method for Continuous Operation of Supported Liquid Membranes, *ibid.*, **20**, 326 (1987).
45) Y.Marcus & A.S.Kertes; "*Ion Exchange and Solvent Extraction of Metal Compleses*", Chapter **10**, Wiley-Intersci. (1969).
46) K.Takahashi, F.Ohtsubo & H.Takeuchi: Mean Drop Diameters of W/O- and (W/O)/W-Dispersions in an Agitated Vessel, *Kagaku Kogaku Ronbunshu*, **6**, 651 (1980).
47) K.Watanabe & H.Takeuchi; Phase Inversion Behavior of Stirred Liquid-Liquid Dispersion, *ibid.*, **7**, 538 (1981).

48) K.Takahashi, F.Ohtsubo & H.Takeuchi; A Study of a Stability of (W/O)/W-Type Emulsions Using a Tracer Technique, *J. Chem. Eng. Jpn.*, **14**, 416 (1981).
49) K.Takahashi, F.Ohtsubo & H.Takeuchi; Effect of Emulsifying Agent on Extraction Rate of Copper by LIX65N, *Kagaku Kogaku Ronbunshu*, **8**, 399 (1982).
50) T.Kinugasa, K.Watanabe & H.Takeuchi; Effect of Organic Solvent of Liquid Surfactant Membranes, *J. Chem. Eng. Japan*, **22**, 593 (1989).
51) T.Kinugasa, K.Watanabe & H.Takeuchi; Stability of (W/O) Emulsion Drops and Water Permeation through its Liquid Membrane in (W/O)/W Dispersion, *ICOM' 90 (Chicago)*, Vol.**1**, p.705 (1990).
52) K.Tsuboi, S.Akita, K.Takahashi & H.Takeuchi; A Study on Water Permeation in (W/O)/W Emulsions, *Kagaku Kogaku Ronbunshu*, **13**, 110 (1987).
53) S.Matsumoto, T.Inoue, M.Kohda and K.Ikura; Water Permeability of Oil Layers in W/O/W Emulsions Under Osmotic Pressure Gradients, *J. Colloid Interface Sci.*, **77**, 555 (1980).
54) M.Takahashi, H.Takeuchi & M.Imanaka; Ion Transport through a Liquid Membrane Containing Crown Ether, *Kagaku Kogaku Ronbunshu*, **7**, 494 (1981).
55) N.Matsuura, K.Umemoto and A.Sasaki; Formation Constants of Dibenzo-18-Crown-6 Complexes with Alkali Metal Ions in DMSO, DMF and PC at 25 °C, *Bull. Chem. Soc. Japan*, **49**, 1246 (1976).
56) K.Takahashi, M.Nakano & H.Takeuchi; Cr(VI) Recovery from Sulfuric Acid Solution with Supported Liquid Membrane, *Kagaku Kogaku Ronbunshu*, **13**, 657 (1987).